Chapter 1

Hybrid Segmentation Methods

Celina Imielinska, Yinpeng Jin, Elsa Angelini
Columbia University

Dimitris Metaxas
Rutgers University

Jayaram K Udupa, Ting Chen, Ying Zhuge
University of Pennsylvania

1.1 Introduction

Image segmentation is the process of identifying and delineating objects in images. It is the most crucial among all computerized operations done on images acquired by using an image acquisition device. Any image visualization, manipulation, and analysis tasks require directly or indirectly image segmentation. In spite of several decades of research [76, 87], this still largely remains an open problem. It is the most challenging among all operations done on images such as interpolation, filtering, and registration. Since these latter operations require object knowledge in one way or another, they all depend to some extent on image segmentation.

Methods for performing segmentations vary widely depending on the specific application, imaging modality, body region and other factors. There is currently no single segmentation method that can yield acceptable results

for every medical image. Combining several segmentation techniques together to form a hybrid framework can sometimes significantly improve the segmentation performance and robustness comparing to each individual component. The hybrid segmentation approach integrates boundary-based and region-based segmentation methods that amplify the strength but reduce the weakness of both approaches. However, most previous work still requires significant initialization to avoid local minima. Furthermore, most of the earlier approaches use prior models for their region-based statistics, which we would rather avoid to increase usefulness in situations where a comprehensive set of priors may not be available. Although this area of research is in its infancy, several promising strategies have been reported. These pioneering methods include: utilizing the results of region-based approach to assist in boundary finding [14, 15, 16, 17, 20, 21, 81, 94], and combining fuzzy connectedness and deformable boundary approaches [45, 56, 57, 58, 90].

We propose a *Hybrid Segmentation Engine* that consists of component modules, for automated segmentation of radiological patient and the Visible Human data. We integrate boundary-based and region-based segmentation methods to exploit the strength of each method hopefully to cover the weakness of the other method. This powerful and promising approach combines fuzzy connectedness (FC) [113, 114], Voronoi Diagram classification method [7, 51], Gibbs prior models (GP) [38] and the deformable models (DM) [66], that constitute respective components of the engine. Each of the component modules in the engine represents a stand-alone segmentation method, but the possibility and advantages of combining the modules in a cooperative fashion, irrespective of the class they represent, may improve performance. We can derive a large number of hybrid segmentation methods by integrating different subsets of the modules, and tailor them to serve the best a specific medical imaging application. Although this area of research is in its infancy, the preliminary results are very encouraging. The hybrid segmentation engine has been fully developed under the NLM funding for Visible Human Project Segmentation and Registration Toolkit Insight Toolkit (www.itk.org). In this chapter we describe one instance of such a hybrid method that combines fuzzy connectedness, Voronoi Diagram classification and deformable models (FC-VD-DM), and Gibbs Prior with Deformable Models (GP-DM) and test them on a number of clinical data sets and the Visible Human data [110].

The following is the organization of the chapter. In the next section, we overview the image segmentation methods and present the rationale for proposing the hybrid segmentation engine. Subsequently, in following three

sections, we describe the hybrid segmentation engine and the hybrid methods derived from it, respectively. In the next section, we describe implementation of the hybrid methods in the itk. The final section contains experimental results that include segmentations of radiological and Visible Human data sets, together with (limited) evaluation of segmentation using quantification of accuracy for true delineation [115].

1.2 Review of Segmentation Methods

For brevity, throughout this paper, we shall refer to any multidimensional vector-valued image as a *scene*, and represent any scene $\mathbf{C}$ by a pair $\mathbf{C} = (C, f)$, where C is a rectangular multidimensional array of volume elements, referred to as *voxels*, and f is a function that assigns a vector to each voxel in C whose components represent imaged property values called *scene intensities*. Scene segmentation may be thought of as consisting of two related processes *recognition* and *delineation*. *Recognition* is the high-level process of determining roughly the whereabouts of an object of interest in the scene. *Delineation* is the low-level process of determining the precise spatial extent and point-by-point composition (material membership percentage) of the object in the scene. Humans are more qualitative and less quantitative. Computers are more quantitative and less qualitative. Incorporation of high-level expert human knowledge algorithmically into the computer has remained a challenge. Most of the drawbacks of current segmentation methods may thus be attributed to the latter weakness of computers in the recognition process. We envisage, therefore, that the assistance of humans, knowledgeable in the application domain, will remain essential in any practical image segmentation method. The challenge and goal for image scientists are to develop methods that minimize the degree of this required help as much as possible. In the following subsections, we shall review the strategies currently available for delineation.

Approaches to delineation are studied far more extensively than those for recognition in image segmentation. In fact, as indicated at the last paragraph, commonly delineation is itself considered to be the entire segmentation process. At the outset, three classes of approaches to delineation may be identified *boundary-based, region-based* and *hybrid* as described below. Boundary-based approaches focus on delineating the interface between the object and the surrounding co-objects in the scene. Region-based approaches

concentrate on delineating the region occupied by the object in the scene. Hybrid approaches attempt to combine the strengths of both boundary-based and region-based approaches. In all three groups, it is possible to use hard (crisp) or fuzzy (in the sense of fuzzy subset theory) strategies to address geometric, shape-related, and topological concepts. In the rest of this section, we shall briefly review these three groups of approaches to delineation.

1.2.1 Boundary-Based Approaches

Mouse-controlled *manual boundary tracing*[112] is the simplest and the most readily available among all delineation methods. Unlike other methods, manual tracing does not require an initial developmental phase (which often can be very time consuming) wherein the method is adapted and fine-tuned to each new application. Major drawbacks of manual tracing, however, are (1) the drudgery and time involved in tracing, and (2) its poor precision, which may vary considerably depending on the fuzziness/sharpness of the boundaries, window level setting used for scene display, brightness/contrast of the monitor, and on the actual size of the object/boundary. First attempts toward automating boundary tracing took *optimum boundary detection* approaches [61, 69, 70, 89], which pose boundary delineation as an optimization problem that is, to pick that among all possible boundaries that can be drawn in the scene which optimizes a properly chosen objective function.

Inadequacies of these methods, especially globally optimal boundaries often differing substantially from the real boundaries, led to the so-called *active contour* or *deformable boundary* methods [24, 25, 39, 59, 62, 64, 65, 66, 72, 119], initiated by the ideas first presented in [59]. In these approaches, an initial boundary is specified somewhat close to the desired boundary (either explicitly by a human operator, or in an implicit fashion such as considering the segmented boundary in the previous slice as the initial boundary for the current slice in a slice-by-slice approach). A mechanical system is then set up to deform the boundary through external forces originating from the scene (such as from scene gradients), through internal forces exerted by the stiffness properties assumed for the boundaries, and external forces specified through user input. The final segmented boundary is taken to be that boundary for which an energy functional is minimized. An advantage of these methods is that, even when boundary information is missing in the scene in some parts of the object boundary, such gaps are filled in simply because of the closure and connectedness properties of the boundary as it is deformed. However,

there is no guarantee that the resulting boundary would match well the real boundary of the object. In an attempt to avoid the post-delineation correction required by these methods, a different family of user-steered delineation methods called live-wire have emerged [34, 35, 36, 71, 105]. In these techniques, recognition by a human operator and delineation by the computer take place cooperatively, synergistically, and with a certain degree of continuity in a tightly coupled manner. By changing this degree, they allow within a single framework various degrees of automation and human interaction. These methods have been shown to be more reproducible and about 3-10 times faster than manual tracing [36] in certain applications and can be quickly (within minutes) adapted to a new application without requiring developmental time [35, 71].

Active shape and appearance methods [26, 27, 28, 29, 33, 43, 67] have emerged recently (and have become popular) in an attempt to overcome some of the inadequacies of the deformable boundary methods. These methods bring in constraints explicitly based on the shape of the boundary as well as the intensity patterns (appearance) in the vicinity of the boundary. The main premise is that, by creating statistical shape and appearance models (in some normalized fashion) for the objects to be segmented in the particular application, and by matching these models through smooth deformation to the information presented in a given scene, the object can be segmented.

Another class of boundary-based delineation techniques called *level-set methods* [63, 74, 106, 107] have emerged also for overcoming the inadequacies of the deformable boundary methods. They have several advantages compared to deformable models. They can handle changing topology naturally, and can deal with local voxel level deformations. In this approach, the boundary of an object is implicitly represented as the zero-level set of a time dependent function called the *level set* function. The manner in which this function evolves over time can be controlled by several entities including the geometric properties of the evolving boundary, scene gradients, and prior boundary shape information. The zero-level set of this function yields the segmentation. Level set methods have been actively pursued in scene segmentation and other applications [55, 106, 107].

1.2.2 Region-Based Approaches

The simplest among region-based methods is intensity thresholding [92]. Many methods to automatically find the thresholds in some optimum fash-

ion have also been devised [1, 60, 75, 99, 102]. Region growing methods [44, 88, 90, 120] evolved in an attempt to overcome the drawbacks of thresholding. The basic idea in region growing techniques is to start from some specified seed voxels and subsequently add voxels in the vicinity of the growing region to the growing region if voxel intensity-based properties satisfy some conditions. If these conditions change adaptively with the growing region, then the repeatability of segmentations with respect to different seed points cannot be guaranteed.

Clustering or *feature space partitioning* methods [30, 32, 111] are among the popular region-based delineation techniques. This is particularly true in brain MR image analysis [9, 12, 22, 40, 48, 68, 84, 85, 86]. The basic premise of these methods is that object regions are manifest as clusters in an appropriate feature space, and therefore, to segment the object regions, we need to identify and delineate the clusters in the scatter plot defined in the feature space. The commonly used clustering methods in medical imaging are k-nearest neighbor [30], c-means [9], and fuzzy c-means [9] techniques. One drawback of clustering techniques as employed commonly is the requirement of multiple (2 or more) features associated with every voxel. In MR image analysis, these are the imaged properties (such as T2, PD, and T1 values). This also implies that the multiple acquisitions should be in registration or should be registered post hoc. Neural network techniques have also been used [42, 83, 93, 102, 120] for the classification of voxels into tissue classes based on the voxels' feature values. *Graph-based approaches* [96, 97, 98, 99, 100, 101, 113, 116, 117, 118, 121], to region delineation pose delineation as a graph problem and present a solution via graph search algorithms. Two actively pursued classes of methods in this group are *graph-cut* [10, 11, 116, 117, 118] and *fuzzy connectedness* [31, 46, 96, 97, 98, 99, 100, 101, 121, 113]. In graph-cut formulation, the scene is represented as a graph with voxels as its nodes and adjacency defining edges. Costs are assigned to edges based on scene intensity properties. A minimum cost cut then generates a segmentation. Such a cut is determined using various types of graph cut algorithms. In fuzzy connectedness, affinity between two nearby voxels defines their local hanging-togetherness in the same object. Affinity is determined based on the distance between voxels as well as on the similarity of their intensity-based features. Fuzzy connectedness is a global fuzzy relation that assigns to every pair of voxels a strength of connectedness which is the strength of the strongest among all paths between the two voxels in the pair. The strength of a path is simply the smallest affinity of pair wise voxels along the path.

Fuzzy connectedness captures the notion of a Gestalt even in the presence of noise, blurring, slow background variation, and natural heterogeneity. The objects are segmented via dynamic programming. The framework has been extended to relative, scale-based, iterative, and vectorial fuzzy connectedness [31, 46, 97, 98, 99, 100, 101, 113, 121], and to a variety of image segmentation applications.

The *Finite Mixture (FM)* model is a commonly used method for statistical scene segmentation because of its simple mathematical formula and the piecewise constant nature of ideal tissue images. However, being a histogram-based model, the FM model has an intrinsic limitation no spatial information is taken into account. Using *Markov Random Field (MRF)*, the spatial information in an image can be encoded through contextual constraints of neighboring voxels [123, 125]. More importantly, *MRF-based* approaches can be combined with other techniques, (e.g., bias field correction) to form an effective approach for tissue segmentation.

Another important class of methods referred to as *watershed* is commonly used for region delineation [104, 101, 95, 82, 80, 8, 6]. In this approach, the n-dimensional scene is considered as a surface in an $(n+1)$-dimensional space. In the 2D scene, the region occupied by an object in the scene is considered to be the set of all those voxels which get flooded under certain conditions when the water level is gradually raised from a starting basin in the surface that corresponds to a set of voxels (seed region) in the object in the scene.

1.2.3 Hybrid approaches

Each of boundary- and region-based approaches has its own strengths and weaknesses. Boundary-based methods are more sensitive to noise than region-based methods. Also, the latter are less affected when high frequency information is missing or compromised in the scene. Further, when the shape of the boundary is extremely complex, model-dependent boundary-based methods run into difficulties. On the other hand, boundary-based methods are better suited for incorporating prior object shape information into delineation as demonstrated by deformable boundary and active shape and appearance methods. They are also less affected by changes in gray level distributions such as those caused by background intensity inhomogeneity [4] and scene-to-scene gray scale variation [73](both are problems encountered in MR image analysis), although region-based methods such as fuzzy connectedness [31, 46, 97, 98, 99, 100, 101, 113, 114, 121] have been shown to be resistant to

these variations. The premise of hybrid methods is to exploit the strength of each method hopefully to cover the weakness of the other method. Although this area of research is in its infancy, several promising strategies have been reported. These methods include: the results of region-based approach to assist in boundary finding [14, 15, 16, 17, 20, 21, 81, 94], combining fuzzy connectedness and deformable boundary approaches [90, 55, 58, 57, 56, 45], and combining fuzzy connectedness with Voronoi-diagram classification method [54, 53, 49, 3].

1.3 Hybrid Segmentation Engine

The Hybrid Segmentation Engine, that has been implemented in the Insight Toolkit (www.itk.org) is an open collection of region and boundary based segmentation methods with its component modules as described in Figure 1.1, namely: Fuzzy Connectedness (FC), Voronoi Diagram classification (VD), Gibbs prior models (GP-MRF), and deformable models (DM). We are capable of generating a large number of hybrid segmentation methods derived from the four modules that can be tailored to a specific medical imaging application and evaluated under a proposed framework for evaluation of segmentation [115]. We show examples, in Figure 1.2, of hybrid methods that we can generate. The modules are implemented in the itk filters. We note that under the FC and DM modules, several different filters have been implemented as it is explained in the next section. Some results using these methods have been already published [121, 100, 49, 53, 55, 54, 3, 18]. [113, 114] and has been successfully used for segmentation of multi-channel images in several applications. This method uses the fact that medical images are inherently fuzzy (inhomogeneous), and we will describe the method in more detail below. In particular, the Fuzzy Connectedness module is implemented under a number of the itk filters for: simple fuzzy connectedness [113, 114], vectorial scale-based fuzzy connectedness [121], vectorial relative fuzzy connectedness [101], and vectorial iterative relative fuzzy connectedness [100]. Boundary-based deformable model module [66] has been implemented in the itk as: 2D and 3D balloon force filters, marching cubes methods to construct deformable meshes close to the object surface, derived from a binary mask of a prior. Region-based Markov Random Field segmentation module that is driven by high order Gibbs prior models has been implemented in the itk to handle single and multi-channel data [125]. Similarly, the Voronoi

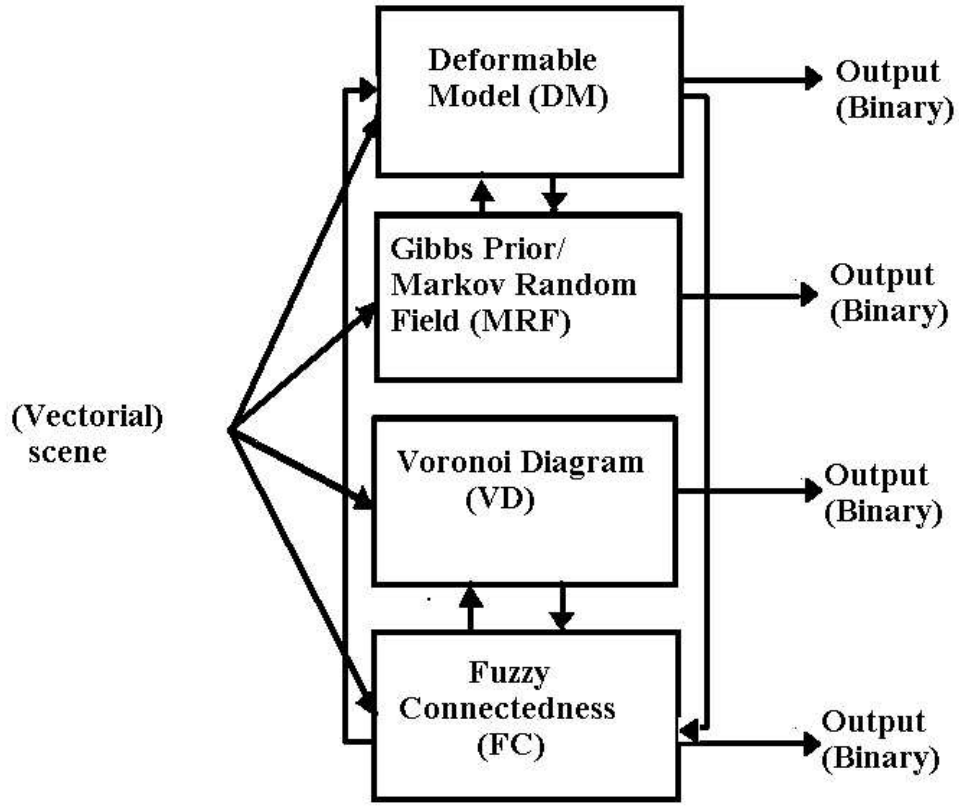

Figure 1.1: The itk-Hybrid Segmentation Engine.

diagram classification has been made available under the itk to handle both single channel and three-channel (RGB and multi-channel radiological) data. In this chapter, we limit our focus to a description of two classes of hybrid methods only, one that integrates fuzzy connectedness (FC), Voronoi diagram classification (VD) and deformable models (VD, and second that integrates Gibbs Prior (GP) with Deformable Model.

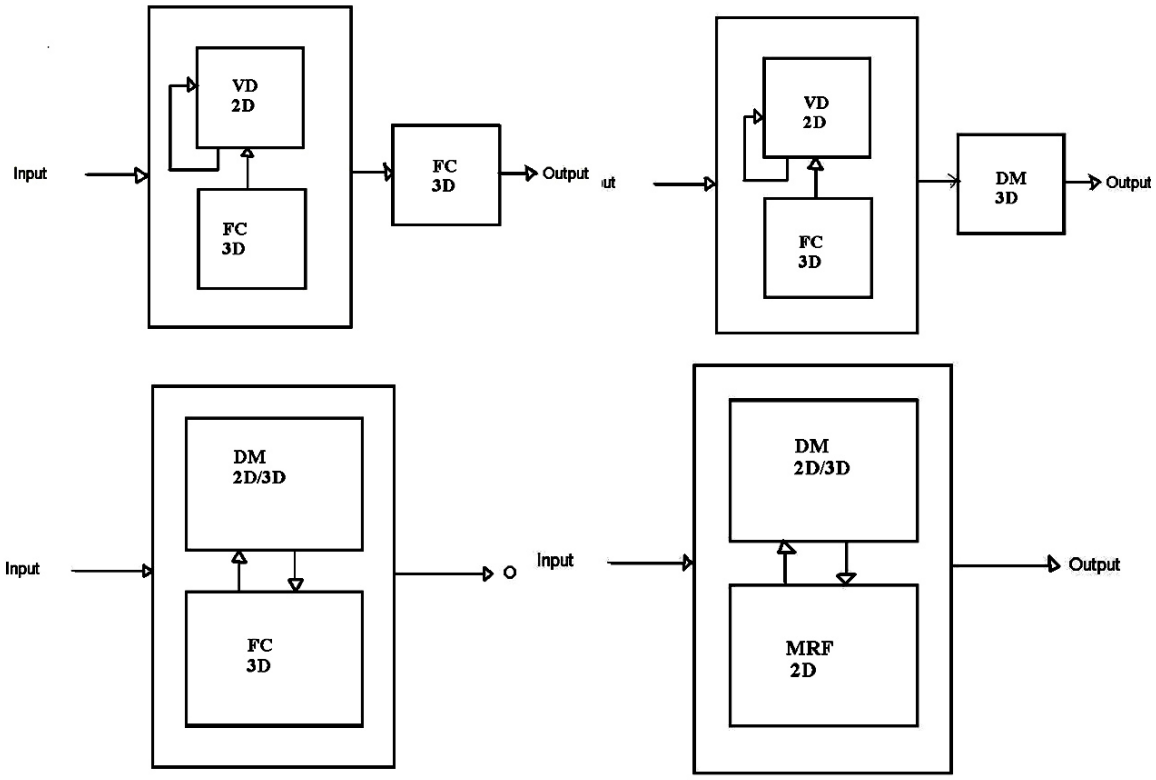

Figure 1.2: Examples of hybrid segmentation methods derived from the itk-hybrid segmentation engine.

1.4 Hybrid Segmentation: Integration of FC, VD and DM

We present a hybrid segmentation method which requires minimal manual initialization, that integrates Fuzzy Connectedness) Fuzzy Connectedness (FC), Voronoi Diagram Classification) Voronoi Diagram Classification (VD) and Deformable Model) Deformable Model (DM). We will start with fuzzy connectedness algorithm to generate a region with a sample of tissue that we plan to segment. From the sample region, we generate automatically homogeneity statistics for the VD classification that will return, in a number of iterations an estimation of the boundary. Below, we describe briefly, the component FC, VD and DM methods.

1.4.1 Fuzzy Connectedness Algorithm (FC)

The simple fuzzy connectedness method, introduced in [114], uses the fact that medical images are inherently fuzzy. We define *affinity* between two *elements* in an image (e.g. pixels, voxels, spels) via a degree of *adjacency* and the *similarity* of their intensity values. The closer the elements are and more similar their intensities are, the greater is the affinity between them. There are two important characteristics of a medical image. First, it has graded composition coming from material, blurring, noise and background variation. Second, the image elements that constitute an anatomical object hang together in a certain way. Both these properties, *graded composition* and *hanging togetherness* are fuzzy properties. The aim of fuzzy connectedness is to capture the global hanging togetherness using image-based local fuzzy affinity.

Let us define a scene over a digital space (Z^n, α) as a pair $\Omega = (C, f)$, where C is an n-dimensional array of spels (elements) and $f : C \rightarrow [0, 1]$. Fuzzy affinity κ is any reflexive and symmetric fuzzy relation in C, that is:

$$\begin{aligned}
&\kappa = \{((c,d), \mu_\kappa(c,d)) | c,d \in C\} \\
&\mu_\kappa : C \times C \rightarrow [0,1] \\
&\mu_\kappa(c,c) = 1, \ for\, all\, c \in C \\
&\mu_\kappa(c,d) = \mu_\kappa(d,c), \ for\, all\, c,d \in C
\end{aligned} \tag{1.1}$$

The general form of μ_κ can be written as follows. For all $c, d \in C$,

$$\mu_\kappa(c,d) = g(\mu_\alpha(c,d), \mu_\psi(c,d), \mu_\phi(c,d), c, d) \tag{1.2}$$

where: $\mu_\alpha(c,d)$ represents the degree of adjacency of c and d, $\mu_\psi(c,d)$ represents the degree of intensity homogeneity of c and d; $\mu_\phi(c,d)$ represents the degree of similarity of the intensity features of c and d to expected object features. Fuzzy κ-connectedness K is a fuzzy relation in C, where $\mu_K(c,d)$ is the strength of the strongest path between c and d, and the strength of a path is the smallest affinity along the path. To define the notion of a fuzzy connected component, we need the following hard binary relation K_Θ based on the fuzzy relation K. Let $\Omega = (C, f)$ be a membership scene over a fuzzy digital space (Z^n, α), and let κ be a fuzzy spel affinity in Ω. We define a (hard) binary relation K_Θ in C as

$$\mu_{K_\Theta} = \begin{cases} 1 & iff\, \mu_\kappa(c,d) \geq \Theta \in [0,1] \\ 0 & otherwise \end{cases} \tag{1.3}$$

Let O_Θ be an equivalence class [123](Chap.10) of the relation K_Θ in C. A *fuzzy κ- component* Γ_Θ *of* C *of strength* Θ is a fuzzy subset of C defined by the membership function

$$\mu_{\Gamma_\Theta} = \begin{cases} f(c) & iff\, c \in O_\Theta \\ 0 & otherwise \end{cases} \tag{1.4}$$

The equivalence class $O_\Theta \subset C$, such that for any $c, d \in C$, $\mu_\kappa(c,d) \geq \Theta$, $\Theta \in [0,1]$, and for any $e \in C - O_\Theta$, $\mu_\kappa(c,d) < \Theta$. We use the notation $[o]_\Theta$ to denote the equivalence class of K_Θ that contains o for any $o \in C$. The *fuzzy κ- component of C that contains, o*, denoted $\Gamma_\Theta(o)$, is a fuzzy subset of C whose membership function is

$$\mu_{\Gamma_\Theta(o)} = \{ \begin{array}{ll} f(c) & iff\, c \in [O]_\Theta \\ 0 & otherwise \end{array} \tag{1.5}$$

A *fuzzy* $\kappa\Theta$*-object of* Ω is a fuzzy κ-component of Ω of strength Θ. For any spel $o \in C$, a fuzzy $\kappa\Theta$-object of Ω that contains o is a fuzzy κ-component of Ω of strength Θ that contains o. Given κ, o, Θ and Ω, a fuzzy $\kappa\Theta$-object of Ω of strength $\Theta \in [0,1]$ containing o, for any $O \in C$, can be computed via dynamic programming [114].

1.4.2 Voronoi Diagram Classification (VD)

This algorithm, which is described in detail in [51], is based on repeatedly dividing an image into regions using VD and classifying the Voronoi regions based on a selected homogeneity classifier for the segmented anatomical tissue. We will use the algorithm as a component in the hybrid method where the classifiers for different tissue type will be generated automatically from the region segmented by the fuzzy connectedness method. VD and Decanal triangulation (DT) play a central role in the algorithm. In 2D, the VD for a set V of points is a partition of the Euclidean plane into Voronoi regions of points closer to one point of V than to any other seed point [91]. For any $p_i \in V$, $V = \{p_1, , p_n\}$, $p_i \in V$, $V = p_1, ..., p_n$

$$VD(p_i) = \{x \in R^2 | d(x, p_i) \leq d(x, p_j), \forall j \neq i, 1 \leq j \leq n \tag{1.6}$$

Similarly, we define the VD in 3D:

$$VD(p_i) = \{x \in R^3 | d(x, p_i) \leq d(x, p_j), \forall j \neq i, 1 \leq j \leq n \tag{1.7}$$

Two Voronoi regions are adjacent if they share a Voronoi edge. The DT, of V is a dual graph of the Voronoi diagram of V, obtained by joining two points whose Voronoi regions are adjacent.

1.4.3 Deformable Model (DM)

3D deformable models used in [127], [128], [129] and [126] are defined as models whose geometric forms (usually are deformable curves and surfaces) deform under the influence of internal and external forces. There are two major classes of 3D deformable models: explicit deformable models ([127], [128], [130] and [129]) and implicit deformable models ([131], [**?**], [133] and [134]).

Although these two classes of models are different at the implementation level, the underlying principles are similar.

Explicit deformable models construct deformable surfaces explicitly using global and local parameters during the segmentation process. One can control the deformation process by changing the values of parameters or using user-defined external forces. Explicit deformable models are easy to represent and faster in implementation. However, the adaptation of model topology is difficult.

Implicit deformable models in [131] represent the curves and surfaces implicitly as a level set [106] of higher-dimensional scalar function. Implicit deformable models can have topological changes during the model deformation. However, the description of implicit deformable models is more complicated and the deformation process takes more time.

There are two different formulations for explicit deformable models: the energy-minimization formulation [59] and the dynamic-force formulation [24] [25]. The energy-minimization formulation has the advantage that its solution satisfies a minimum principle; while the dynamic force formulation provides the flexibility of applying different types of external forces onto the deformable model. In dynamic force formulation models, external forces push the model to the features of interest in the image and the model stops when these external forces equilibrate or vanish. The external forces can be potential forces, non-potential forces such as balloon forces, and the combination of both. Potential forces are derived from image information, e.g. the gradient information. They can attract the deformable model to the boundary of the object or other features of interest in the image. The balloon force was proposed by Cohen [24]. In [24] the deformable model starts as a small circle (2D) or sphere (3D) inside the object. The balloon force can help to push the model closer to the boundary by adding a constant inflation force inside the deformable model. Therefore the balloon-force-driven deformable model will expand like a balloon being filled with gas. However, for objects with complex surface structures, the deformable model may leak out of the boundary if it uses the balloon force exclusively. In medical imaging applications, we usually use the combination of both forces to achieve a better deformation performance.

In our framework, we use the dynamic force formulation of the explicitly parameterized deformable model. The deformable model has a simple description, easy to be interacted with, and can segment the object of interest with high efficiency. We use other modules in the hybrid framework to lead

it out of local minima during segmentation process.

Traditional deformable models such as snakes and balloons fail to segment 3D objects with complex surface structures. In [66] we use a super-quadric ellipsoid model which is capable of performing global and local deformation using tapering, bending, and twisting parameters. Nonetheless, it is difficult for this model fit to objects with deep concavities on their surface and the final segmentation result may be over smoothed. Instead of using extensive user-defined constraints and external forces on the model surface, we try to initialize the geometry of the deformable model close enough to boundary features so that the gradient derived forces can directly lead the model to the object surface. This gives us the motivation of integrating the marching cubes method [136] [135] into our framework.

We use the marching cubes method to create a surface mesh based on the 3D binary mask created by a prior model. We define a voxel in a 3D binary image volume as a cube created from 8 pixels, four each from a slice. We give an index to the 13 potential locations of nodes on the deformable model surface in this cube and define 13 possible plane incidences onto which elements of the deformable model can lie.

Given that the binary mask is close enough to the surface of the object, the mesh created by the march cubes method should be in the effective range of the gradient force. One can use this mesh as the initial deformable surface and apply gradient derived forces onto it from the very beginning of the fitting process. By doing so, the deformable model can fit well into concavities and convexities on the object surface. Plus, we skip the balloon fitting process so that the deformation process is shortened.

There are several other advantages in using the marching cubes method for 3D deformable mesh construction. The deformable surface created by the marching cubes method is close to the object surface so that we can assume that the global displacement is small enough to be neglected during the deformation. Therefore we only need to consider the local displacement during the deformable model fitting process. The deformable mesh created by the Marching Cubes method is composed of sub-pixel triangular elements. Therefore the final segmentation result can also achieve sub-pixel accuracy.

To integrate fuzzy connectedness, Voronoi diagram classification and the deformable model into a hybrid segmentation method, we must fit the result of the Voronoi diagram classification into the deformable model. For a 3D segmentation task, the marching cubes method [124] s used to create an initial 3D deformable model surface, from a prior 3D binary mask. A mesh

surface is constructed that is close enough to the actual surface of the object [125]. From the mesh, a 3D deformable model is created and a combination of the edge force and the gradient-based force is applied to the deformable model to improve the segmentation result, for more details see [125].

1.4.4 The Hybrid Method: Integration of FC, VD and DM.

The algorithm integrates two methods, the fuzzy connectedness and VD-based algorithm. We will outline the algorithm first, and explain the component steps later. The fuzzy connectedness algorithm is used to segment a fragment of the target tissue. From the sample, a set of statistics is generated automatically, in RGB and HVC color spaces, to define the homogeneity operator. The homogeneity operator will be used as a multi-channel classifier for the VD-based algorithm. As we mentioned, we will use, in the future, the deformable model, to determine the final (3D) smooth boundary of the segmented region. Below, we outline the hybrid method:

Step 1. We run the fuzzy connectedness algorithm to segment a sample of the target tissue, and generate statistics, average and variance, in three color channels, in two color spaces, RGB and HVC.

Step 2. Run the VD-based algorithm using multiple color channels, until it converges:

(a) For each Voronoi region, classify it as interior/exterior/boundary region using multi-channel homogeneity operator;

(b) Compute DT and display segments which connect boundary regions;

(c) Add seeds to Voronoi edges of Voronoi boundary regions;

(d) Go To Step 2(a) until the algorithm converges to a stable state or until the user chooses to quit.

Step 3. (optional) Use the deformable model to determine the final (3D) boundary and re-set the homogeneity operator.

Implementation of Step 1. To initialize the fuzzy connectedness algorithm and establish the mean and standard deviation of voxel values and

their gradient magnitudes, the user collects the pixels within the region of interest, by clicking on the image and selecting at each time a square region with 5×5 pixels. Then an initial seed voxel is selected to compute the fuzzy connectedness, using the dynamic programming approach [113, 115]. We determine the strength of the fuzzy connectedness Θ, $\Theta \in [0, 1]$, by letting the user to select interactively its threshold value, such that the initially segmented sample of the target tissue resembles the shape of the underlying image. For a binary image with a roughly segmented sample of a tissue, we generate the strongest three channels in two color spaces, RGB and HVC [41], for average and variance, respectively. First, we define for the binary image, the smallest enclosing rectangle, a region of interest (ROI), in which we identify the segmented image and its background. Within the ROI, we calculate the mean and variance in each of the six color channels (R,G,B,H,V,C) for the object and its background, respectively. Then three channels with the largest relative difference in mean value and in variance value between the object and its background are selected, respectively. The homogeneity operator for the VD-based algorithm uses the expected mean/variance values of the object together with tolerance values, computed for each selected channel, for classifying the internal and external region Implementation of Step 2. We build an initial VD by generating some number of random seed points (Voronoi points) and then run the QuickHull, [5], to calculate the VD. Once the initial VD has been generated, the program visits each region to accumulate classification statistics and makes a determination as to the identity of the region. For each Voronoi region, the mean/variance value for the pre-selected channels are computed, if they are similar, then it is marked as internal, otherwise external. Those external regions that have at least one internal neighbor are marked as boundary. Each boundary region is divided for next iterations until the total number of pixels within it is less than a chose number. We will describe below, the itk toolkit implementation section, other hybrid methods that can be derived from these three: FC, VD and DM modules.

1.4.5 Hybrid Segmentation: Integration of Gibbs Prior Model and Deformable Model.

The integration of Gibbs prior with Deformable Models has been described in the chapter discussing the Gibbs prior.

1.5 Evaluation of Segmentation

A complete description of the evaluation framework for segmentation can be found in [115]. We will outline the main points of this approach and demonstrate using this framework in a limited fashion (namely for assessment of accuracy of delineation) in our preliminary studies. For evaluating segmentation methods, three factors - *precision* (reproducibility), *accuracy* (agreement with truth, validity), and *efficiency* (time taken) need to be considered for both recognition and delineation. To assess precision, we need to choose a figure of merit, repeat segmentation considering all sources of variation, and determine variations in figure of merit via statistical analysis. It is impossible usually to establish true segmentation. Hence, to assess accuracy, we need to choose a surrogate of true segmentation and proceed as for precision. In determining accuracy, it may be important to consider different "landmark" areas of the structure to be segmented depending on the application. To assess efficiency, both the computational and the user time required for algorithm and operator training and for algorithm execution should be measured and analyzed. Precision, accuracy, and efficiency are interdependent. It is difficult to improve one factor without affecting others. Segmentation methods must be compared based on all three factors. The weight given to each factor depends on application. Any method of evaluation of segmentation algorithms has to, at the outset, specify the application domain under consideration. We consider the application domain to be determined by the following three entities: A: An application or task; example: volume estimation of tumors; B: A body region; example: brain; P: An imaging protocol; example: FLAIR MR imaging with a particular set of parameters. An evaluation description of a particular algorithm α for a given application domain $< A, B, P >$ that signals high performance for α may tell nothing at all about α for a different application domain $< A', B', P' >$. For example, a particular algorithm may have high performances in determining the volume of a tumor in the brain on an MR image, but have low performance in segmenting a cancerous mass from a mammography scab if a breast. Therefore, evaluation must be performed for each application domain separately. The following additional notations are needed for our description.

Object: A physical object of interest in B for which images are acquired; example: brain tumor.

Scene: A 3D volume image, denoted by $=(C, f)$, where C is a rectangular array

of voxels, and $f(c)$ denotes the *scene intensity* of any voxel $c \in C$. C may be a vectorial scene, meaning that $f(c)$ may be a vector whose components represent several imaged properties. C is referred to as a binary scene if the range of $f(c)$ is $\{0, 1\}$.

S: A set of scenes acquired for the same given application domain: $< A, B, P >$.

In this section, we will evaluate segmentation methods using assessment of accuracy of true delineation by comparing true delineation of the scenes with the one obtained by a segmentation algorithm. Thus, we will not address the other two factors, precision and efficiency, but we have to note that these factors are extremely important. A complete evaluation of segmentation methods under all three factors must be done under precisely defined experiments, where the acquired data and collection of true delineation and true recognition is done following strict protocols, a task that we were not able to fulfill under the itk project. For patient images, since it is impossible to establish absolute true segmentation, some surrogate of truth is needed. We will use manual delineation where the object boundaries are traced or regions are painted manually by experts.

Let S_{td} be the set of scenes containing true delineations for the scenes in S. For any scene $C \in S$, let C_o^M be the scene representing the fuzzy object defined by an object o of B in C obtained by using method M, and let $C_{td} \in S_{td}$ be the corresponding scene of true delineation, all under the application domain $< A, B, P >$. The following measures are defined to characterize the accuracy of method M under $< A, B, P >$ for delineation.

False Negative Volume Fraction: $FNVF_M^d(o) = \frac{|C_{td} - C_o^M|}{C_{td}}$

False Positive Volume Fraction: $FPVF_M^d(o) = \frac{|C_o^M - C_{td}|}{|C_{td}|}$

True Positive Volume Fraction: $TPVF_M^d(o) = \frac{|C_o^M \bigcap C_{td}|}{|C_{td}|}$

The meaning of these measures is illustrated in Figure 1.3 for the binary case. They are all expressed as a fraction of the volume of true delineation. $FNVF_M^d$ indicates the fraction of tissue defined in C_{td} that was missed by method M in delineation. $FPVF_M^d$ denotes the amount of tissue falsely identified by method M as a fraction of the total amount of tissue in C_{td}. $TPVF_M^d$ describes the fraction of the total amount of tissue in C_{td} with which the fuzzy object C_o^M overlaps. Note that the three measures are independent; that is; none of them can be derived from the other two. True negative

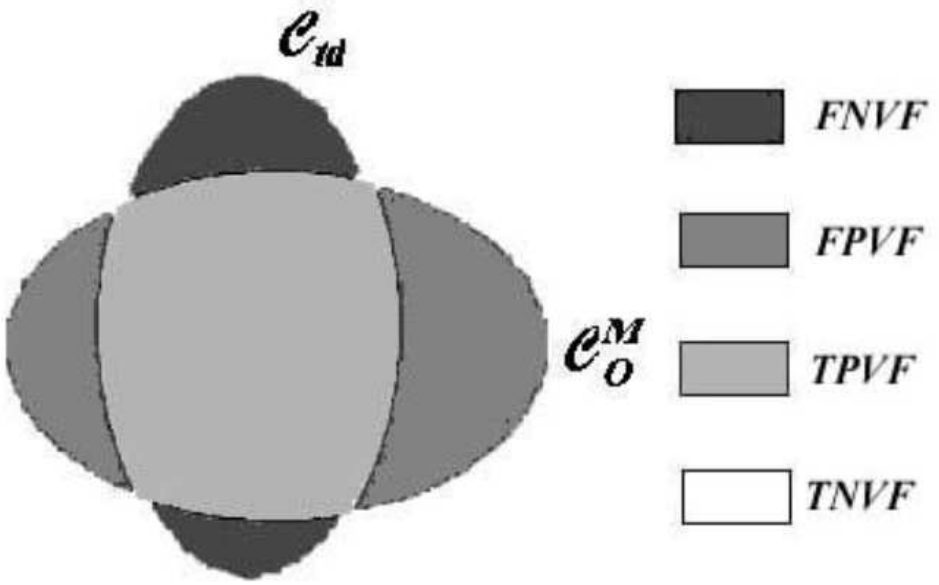

Figure 1.3: A geometric illustration of the three precision factors for delineation.

volume fraction has no meaning in this context since it would depend on the rectangular cuboidal region defining the scene domain C.

We will use this limited version of the evaluation framework in assessing the accuracy of segmentation compared with true delineation in some examples presented below.

1.6 Results

We have demonstrated capabilities of the method in segmentation of various organs and tissues and our results are promising. The hybrid methods that are derived from the hybrid segmentation engine has been shown effective in delineating even complex heterogeneous anatomical tissue. We present results that involve both the Visible Human data and radiological patient data that have been segmented under a number of different projects. Some of the results were evaluated for accuracy of delineation using quantified

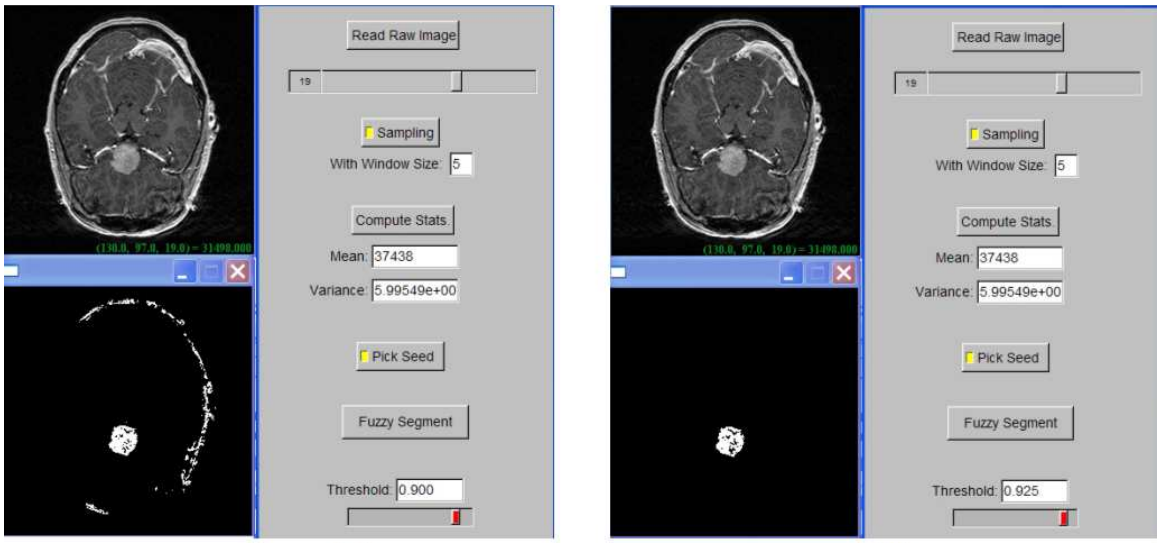

(a) (b)

Figure 1.4: Fuzzy segmentation of a brain tumor from a patient MRI data, with FC threshold (a) 0.9, and (b) 0.925.

measures from our proposed framework for evaluation of segmentation.

1.6.1 Segmentation of Brain Tumor from MRI data.

We have recently processed the radiological imaging data from a patient who underwent an orbito-zygomatic craniotomy for the removal of an anterior skull base meningioma. The following example shows this patients MRI data that has been segmented with FC segmentation, Figure 1.4, using two different parameters for the strength of FC segmentation. In Figure 1.5, we overlay the segmented 3D tumor on intraoperative digital photographs obtained through the operating microscope during critical portions of the procedure. These are preliminary results for a project, being developed at Columbia University Department of Neurological Surgery, to apply augmented reality for microscope guided skull base surgery.

1.6.2 Segmentation of Visible Human Data

We have developed at Columbia electronic atlases [50] from the Visible Human [110] data sets that are systematically incorporated into the anatomy

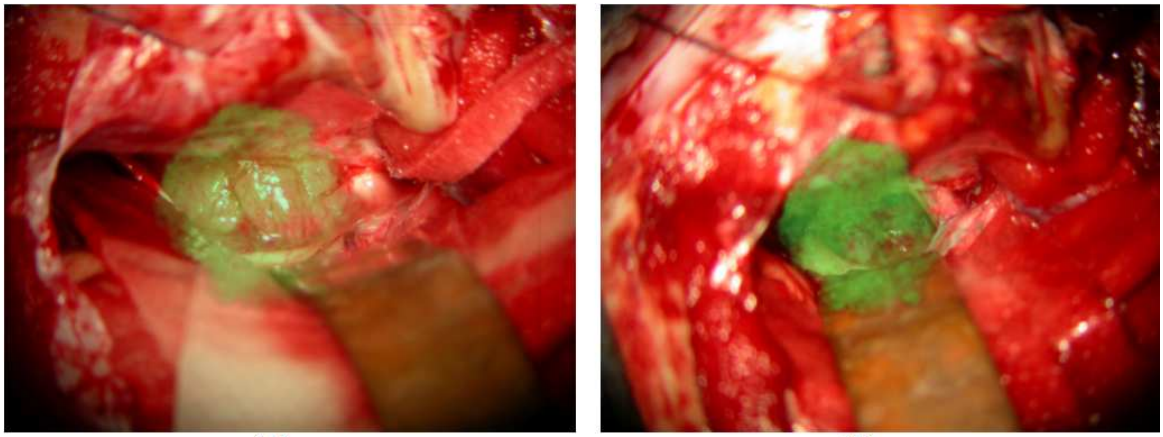

(a) (b)

Figure 1.5: 3D model of the tumor overlaid over two snapshots from a surgery for the removal of an anterior skull base meningioma: (a) before and (b) after tumor removal. (Courtesy to Dr. J. Bruce and Dr. A. DAmbrosio)

curriculum at Columbia University College of Physicians and Surgeons. We have tested our segmentation methods on the color Visible Human data and compared the results with the hand segmentations delineated by an anatomy expert. In Figure 1.6 we show segmentation of the temporalis muscle using FC/VD segmentation. In Figure 1.6, we illustrate steps of the FC/VD method, where Figure 1.6 (b) shows a sample tissue segmented with FC method, and from this sample we derive homogeneity operator to classify Voronoi region in the VD classification. In Figure 1.6 (c)-(g), we show iterations of the VD classification, with the yellow boundary Voronoi regions that converge into the final boundary of the segmented region. Finally, in Figure 1.6 (h) we outline the boundary with a subgraph of the Decanal triangulation, a dual graph to Voronoi diagram.

In Figure 1.7, we use FC/VD segmentation to delineate visceral adipose tissue, that is highly heterogeneous, in the abdomen region.

In Figure 1.8, we segmented left kidney from the Visible Human Male data set set using: FC, Figure 1.8(b); FC/VD followed by a selection of a connected component, Figure 1.8(c); and FC/VD/DM, Figure 1.8 (d); and in Figure 1.9 we show corresponding 3D models generated with our in-house 3D Vesalius Visualizer.

We compared the results for FC, FC/VD, and FC/VD/DM with hand seg-

mentation of the left kidney using accuracy assessment for true delineation. In Figure 1.10 we present the quantified accuracy errors. The result shows that the VD classification improves the FC segmentation, and DM calibrates the final segmentation. It also shows that we can make a fair comparison of accuracy of successive segmentation steps using quantified parameters, while it is impossible to assess the same error by mere observation.

1.6.3 3D Rotational Angiography.

In Figure 1.11 and Figure 1.12, we present segmentation of 3D rotational angiogram data that is processed by fuzzy connectedness (FC) and fitted with deformable model and the corresponding 3D model.

1.6.4 Quantification of Adipose Tissue from Whole Body MRI Scans

One of our collaborative projects, with Dr. Heymsfield, the Director of the St. Lukes Roosevelt Obesity Research Center, involves quantification of adipose tissue from whole body MRI scans. We are in a process of building an integrated system for acquisition, imaging, reconstruction and quantification of body composition. The existing approach at the Center uses manual segmentation of the adipose and other tissue from the MRI scans, a very time consuming and laborious process. The outcome of manual segmentations and corresponding 3D visualizations are presented in Figure 1.13(a) and (b). We used FC/VD hybrid segmentation on a data set that is a scan of an abdomen that consists of 6 slices in the volume, and the preliminary results are promising. We used the existing 16 manual segmentations that have been collected over time from a number of experts working for the Center who were asked to segment the same MRI scan of an abdomen, and to repeat the same segmentation three times in three month-intervals. We used these manual segmentations as a source for deriving true delineation of adipose tissue. In Figure 1.14 and Figure 1.15 we show intra- and inter- operator variability for the manual segmentations, respectively. We must note that even though the protocol for the manual segmentations was well specified, we cannot say that was fully controlled. We are know that this is not a perfect set manual delineations, yet we used it to derived true delineation to conduct quantification of accuracy. We use the from the evaluation framework, as reported in [115]. Below, we present results from the steps of our hybrid method. In Figure

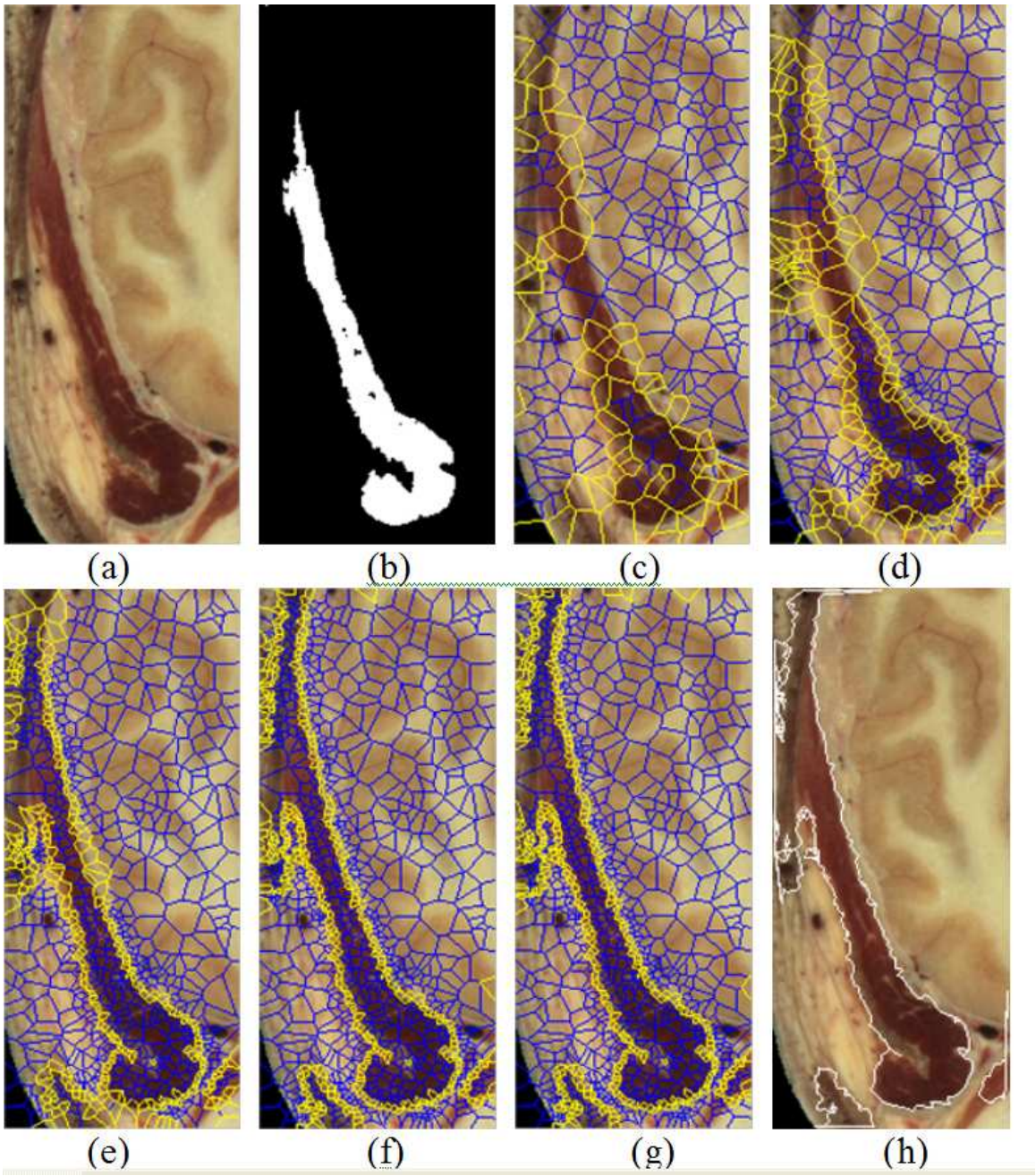

Figure 1.6: Automated segmentation of temporalis muscle: (a) color Visible Human Male slice, (b) a fuzzy connected component, (c)-(g) iterations of the VD-based algorithm , (g) an outline of the boundary.

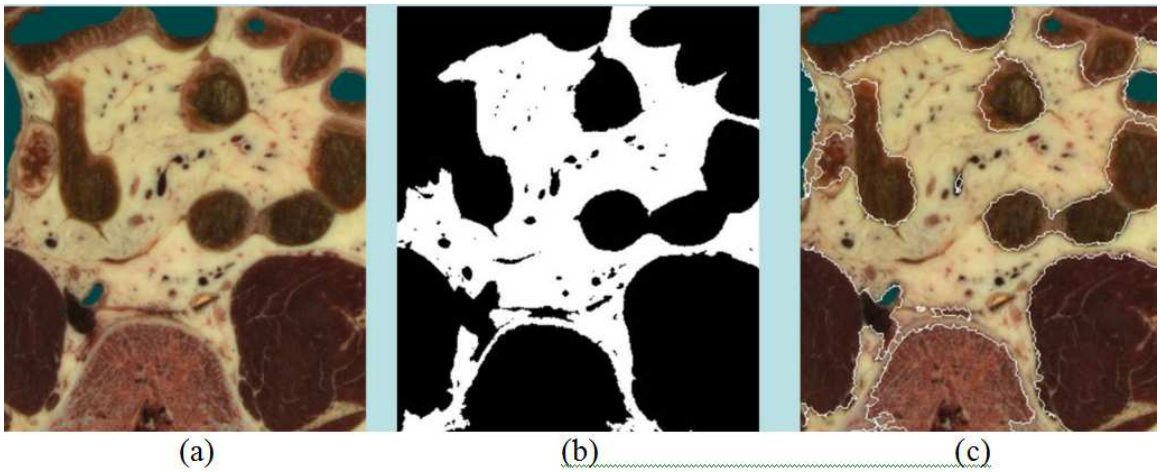

Figure 1.7: FC-VD Segmentation of Visible Human Male adipose tissue in the abdomen region. (a) input data, (b) FC, (b) VD final boundary.

1.16 we show the input slice, the fuzzy map, and the FC segmented region with user selected fuzzy connectedness value. In Figure 1.17, we segment visceral and subcutaneous tissue using FC-VD segmentation, followed by a basic smoothing of the segmented region.

Below, we present accuracy quantification using parameters in equations comparing the outcome of FC/VD segmentation with the true delineation. In Figure 1.18, we show three out of 6 slices from our input data set. The true delineation was established by averaging sixteen manual delineations in a form of corresponding binary masks into a fuzzy object (with pixel values between 0 and 1), for details, see [115]. The results of segmentation of the data with FC/VD were compared with the true delineation. The three factors (FNVP, FPVF, TPVF) for measuring the accuracy of true delineation for individual slices in the data (the inter-slice distance in the data set was too large to treat as a contiguous volume) are computed. We observe, in Figure 1.19 that the simple measurement of area difference does not provide accurate evaluation in terms of overall performance, while parameters (FNVP, FPVF, TPVF) give better characterization of the accuracy measurement.

Our segmentation system gives in general 8% 9% accuracy in these slices, comparing to the best possible accuracy of 5% -7% from Figure 1.19. As for the efficiency measurement, an experienced human operator usually takes about $15 - 20$ minutes to finish a delineations session on adipose tissue for a

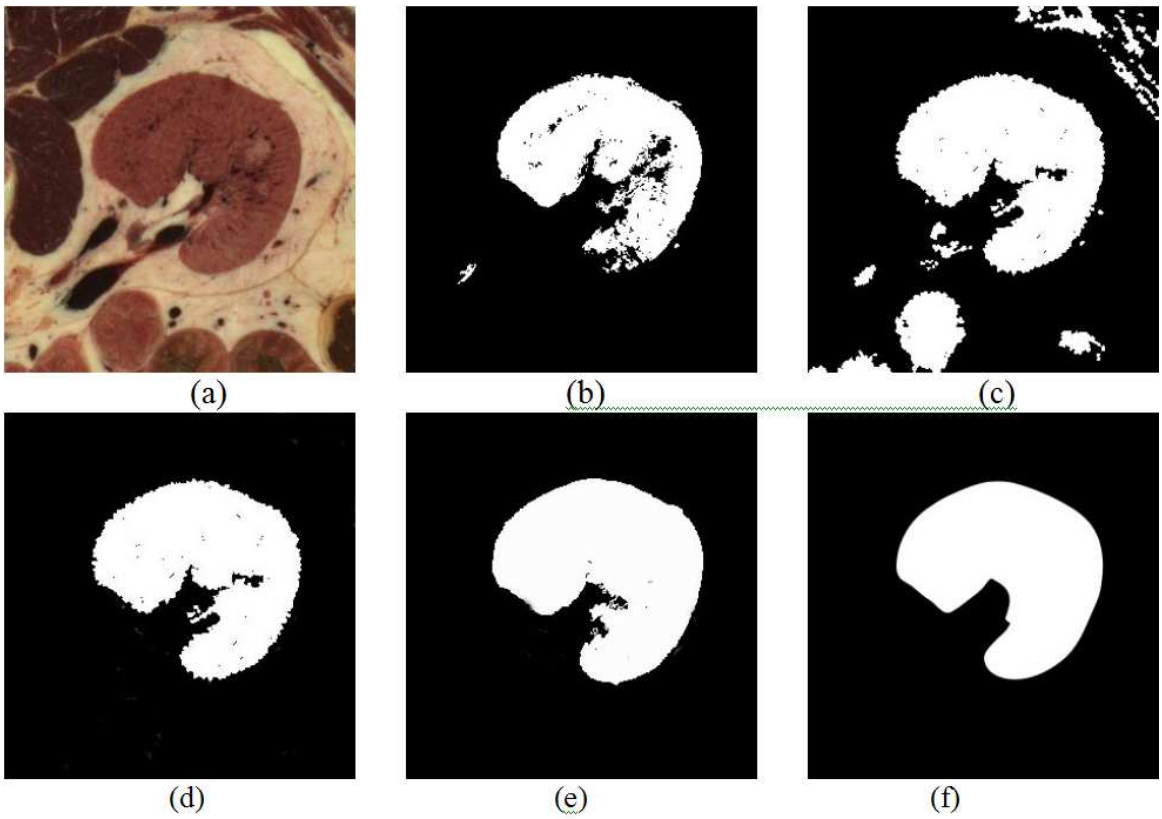

Figure 1.8: Segmentation of the Visible Human Male left kidney. (a) input data, (b) FC, (c) VD, (d) VD-CC, (e) DM, (f) hand segmentation.

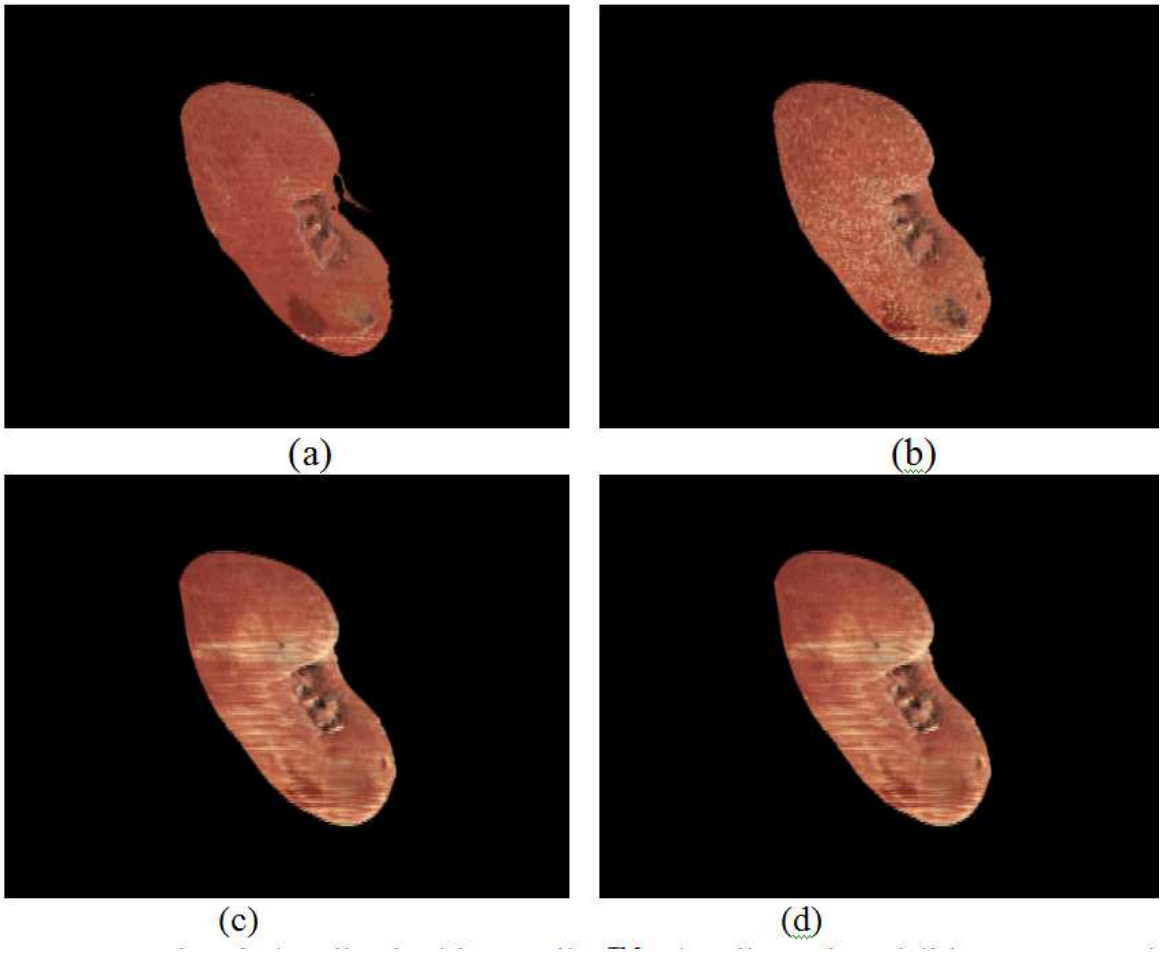

Figure 1.9: 3D segmented and visualized with $Vesalius^{TM}$ Visualizer, the Visible Human Male left kidney. 3D models of: (a) FC, (b)VD-CC, (c) DM, (d) hand segmentation.

	FZ	VD-CC	DM
Area Difference (%)	17.2	5.6	0.91
FNVF	0.193	0.084	0.053
FPVF	0.021	0.028	0.062
TPVF	0.807	0.916	0.947

Figure 1.10: Visible Human male: kidney. Quantification of accuracy for true delineation.

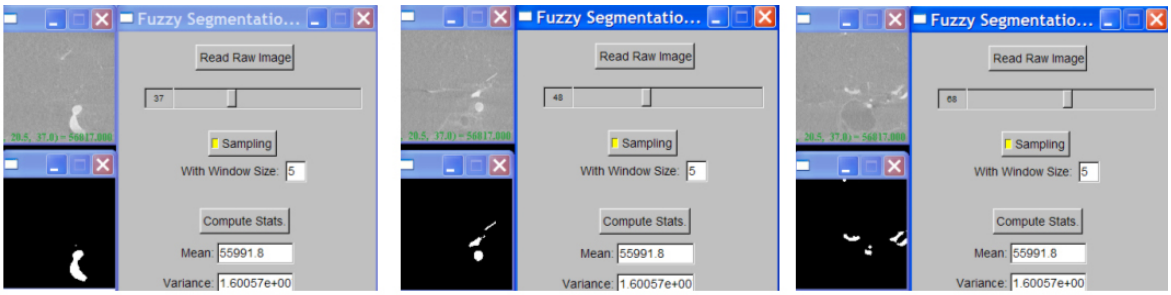

(a) (b) (c)

Figure 1.11: 3D rotational angiogram data segmented with fuzzy connectedness algorithm: (a)-(c) three segmented slices in the volume.

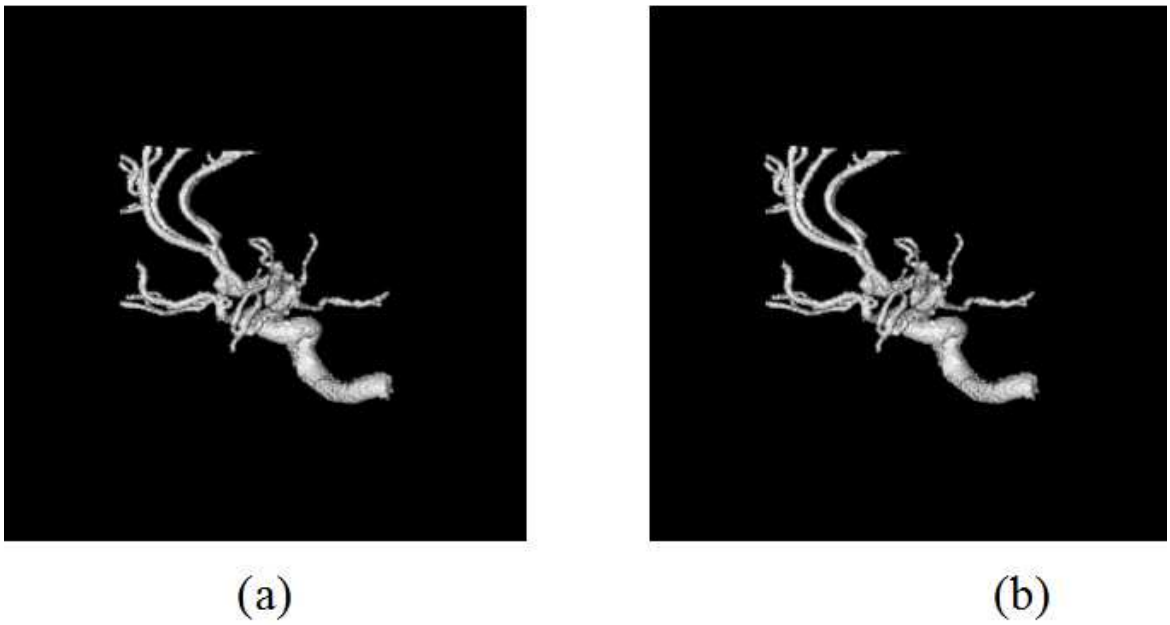

Figure 1.12: 3D rotational angiogram, segmented with (a) FC, and (b) finished with DM segmentation.

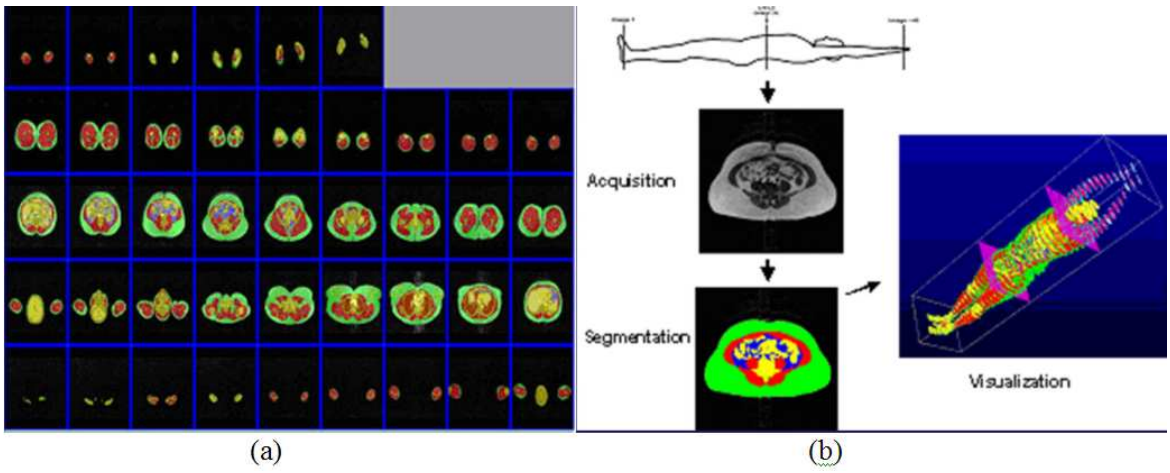

Figure 1.13: Obesity Research Center Integrated system for quantification of Adipose tissue from Whole Body MRI scans. Courtesy of Dr.Heymsfield.

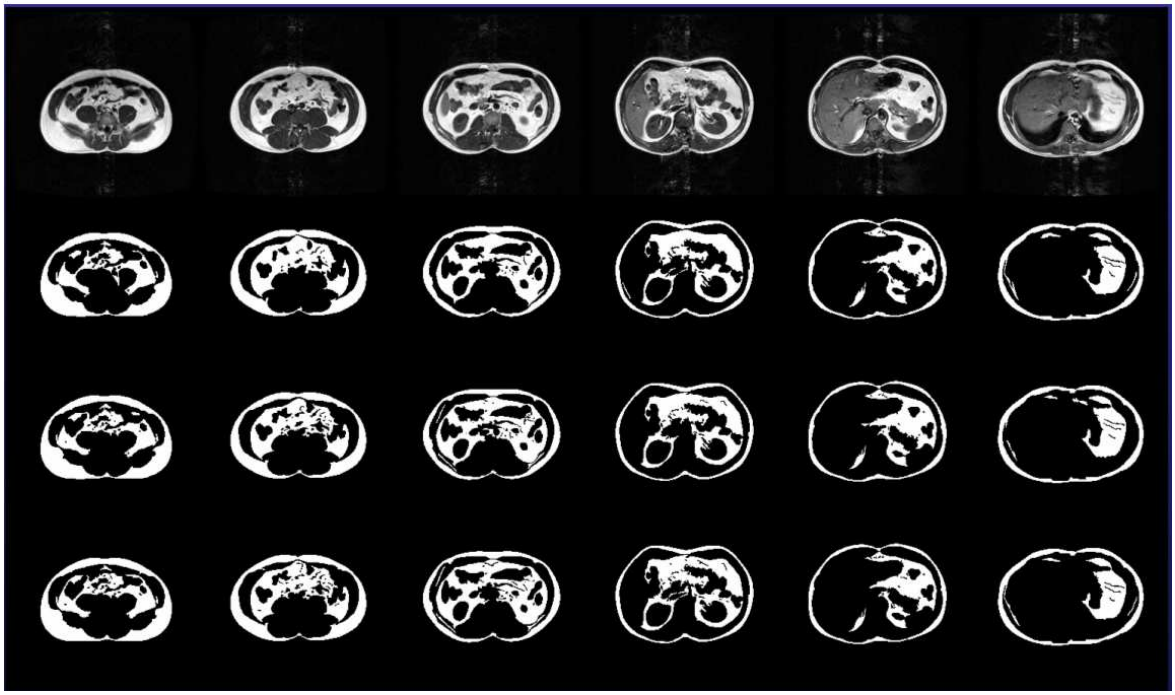

Figure 1.14: Quantification of adipose tissue from whole body MRI T1 weighted scans- 6 slices from the abdomen. Evaluation of accuracy of segmentation ground truth (delineation) intra-operator variability.

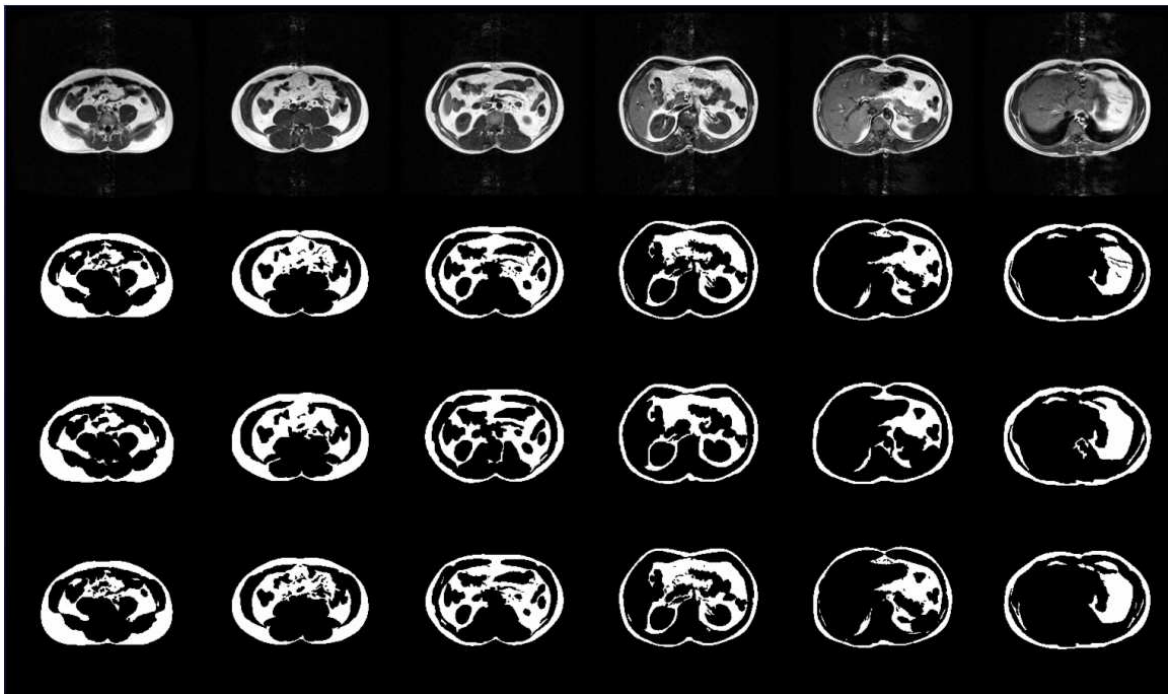

Figure 1.15: Quantification of adipose tissue from whole body MRI T1 weighted scans- 6 slices from the abdomen. Evaluation of accuracy of segmentation ground truth (delineation) inter-operator variability.

Figure 1.16: Fuzzy Connectedness Segmentation. (a) Input image. (b) Fuzzy Scene Map. (c) Result: segmented object with fuzzy connectedness level value (a user-defined threshold) of 0.025.

Figure 1.17: Quantification of adipose tissue from whole body MRI scans. (a) Input data MRI T1 image, (b) Training (simple FC), (c) Segmented Image VD classification, (d) Smoothed segmented image visceral and subcutaneous tissue.

7-slice MRI T1 data set. While using our semi-automatic system, only a few mouse-clicks are needed, and the segmentation for 2D slice image is usually finished in real time (less than 1 second).

1.7 Conclusions.

We have proposed a Hybrid Segmentation Engine with its component modules that are boundary-based and region-based segmentation methods implemented in the itk. From the Engine, we can derive a number of hybrid methods that integrate boundary- and region- based approach to segmentation into powerful new tools that exploit the strength of each method and hopefully cover the weaknesses of the other method. In particular we presented an instance of a hybrid method that combines the fuzzy connectedness, Voronoi diagram classification and deformable models and tested it on the Visible Human and radiological patient data. In some examples, like the quantification of adipose tissue from whole body MRI scans, we have quantified accuracy error for true delineation using three factors: FNVP, FPVF, TPVF. Under the framework, we have demonstrated that the results from the hybrid segmentation methods are close to those obtained from manual delineations (surrogates of ground truth). Although this area of research is still in its infancy, the preliminary results are very encouraging, and hybrid segmentation methods have a potential to become important tools in medical

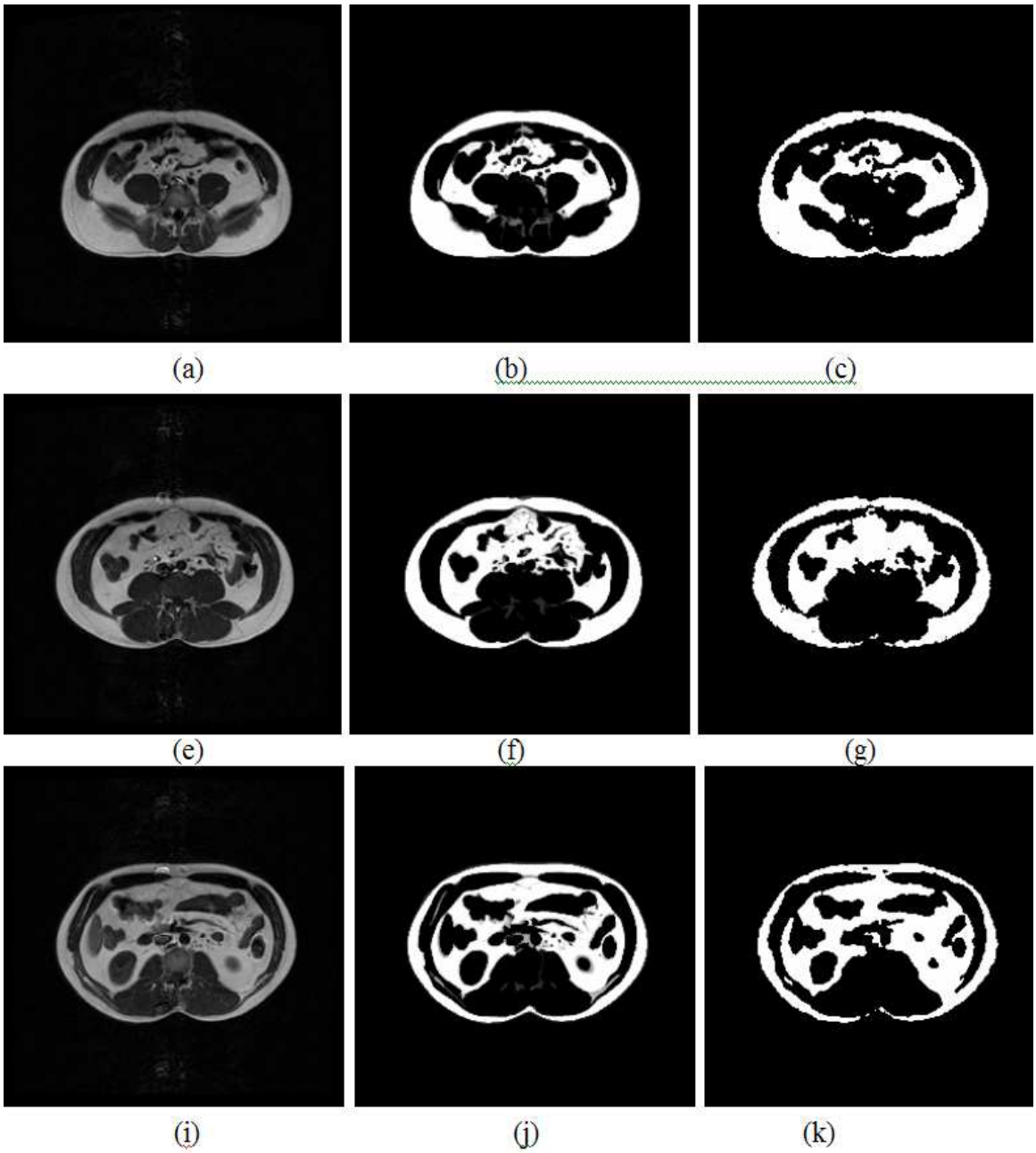

Figure 1.18: Results depicting hybrid and manual segmentation: (a)(e)(i) input images (MRI T1); (b)(f)(j): ground truth images; (c)(g)(k): FC/VD hybrid segmentation.

Ground Truth	Area difference (%)	FNVF (%)	FPVF (%)	TPVF(%)
Figure (b)	1.3	8.2	9.4	91.8
Figure (f)	0.2	7.7	7.9	92.3
Figure (j)	3.9	8.1	11.9	91.9

Figure 1.19: Accuracy measurements of the FC/VD segmentation shown in Figure 26(c), (g) and (k).

image processing.

Bibliography

[1] A. Abutaleb, "Automatic thresholding of gray-levelpictures using two-dimensional entropy," *Computer Vision, Graphics*, and Image Processing, 47:22-32, 1989.

[2] D. Adalsteinsson and J. A. Sethian, "A fast level set method for propagating interfaces," *Journal of Computational Physics*, vol. 118, pp. 269-277, 1995.

[3] E. Angelini, C. Imielinska, Y. Jin and A. Laine, "Improving statistics for hybrid segmentation of high-resolution multichannel images," in *Proceedings of SPIE*, 4684:401-411, 2002.

[4] L. Axel, J. Costantini and J. Listerud, "Intensity Corrections in Surface-Coil MR Imaging," *American Journal of Roentgenology*, 148:418-420, 1987.

[5] Barber, C.B.; Dobkin, D.P, Huhdanpaa H.:The Quickhull Algorithm for Convex Hull, The Geometry Center, University of Minnesota, 1995.

[6] S. Beucher and C. Lantuejoul, "Use of watersheds in contour detection," in Proceedings of the International Workshop on Image Processing, Real-Time Edge and Motion Detection/Estimation, 17-21, 1979.

[7] E. Bertin, F. Parazza, and J. M. Chassery, "Segmentation and measurement based on 3D VoronoiDiagram: application to confocal microscopy," *Computerized Medical Imaging and Graphics*, vol. 17, pp. 175-182, 1993.

[8] S. Beucher, "The watershed transformation applied to image segmentation," *10th Pfefferkorn Conference on Signal and Image Processing in Microscopy and Microanalysis*, 299-314, 1992.

[9] J. Bezdek, L. Hall and L. Clarke, "Review of MR image segmentation techniques using pattern recognition," *Medical Physics*, 20:1033-1048, 1993.

[10] Y. Boykov and M. Jolly, "Interactive graph cuts for optimal boundary & region segmentation of objects in N-D images," in *Proceedings of ICCV*, Part I, 105-112, 2001.

[11] Y. Boykov, O. Veksler and R. Zabih, "Fast approximate energy minimization via graph cuts," *IEEE Transactions on Pattern Analysis and Machine Intelligence*, 23:1222-1239, 2001.

[12] M. Brandt, T. Bohan, L. Kramer and J. Fletcher, "Estimation of CSF, white and gray matter volumes in hydrocephalic children using fuzzy clustering of MR images," *Computerized Medical Imaging and Graphics*, 18:25-34, 1994.

[13] I. Carlbom, D. Terzopoulos, K. Harris, "Compute-assisted Registration, Segmentation, and 3D Reconstruction from Images of Neuronal Tissue Sections", IEEE Transaction on Medical Imaging 13(2): 351-362.

[14] A. Chakraborty, L. H. Staib and J. S. Duncan, "Deformable Boundary Finding Influenced by Region Homogeneity", in *Proceedings of Conference of Computer Vision and Pattern Recognition (CVPR'94)* 624-627, Seattle, WA, June, 1994.

[15] A. Chakraborty, Duncan, J.S., Integration of Boundary Finding and Region-Based Segmentation Using Game Theory, In Y. Bizais et al., editor, Information Processing in Medical Imaging, Kluwer, pp.189-201, 1995.

[16] A. Chakraborty, L. Staib and J. Duncan, "Deformable boundary finding in medical images by integrating gradient and region information," *IEEE Transactions on Medical Imaging*, 15:859-870, 1996.

[17] A. Chakraborty, L. Staib and J. Duncan, "An integrated approach to surface finding for medical images," in *Proceedings of IEEE Workshop on Mathematical Methods in Biomedical Image Analysis*, 253-262, 1996.

[18] T. Chen, D. Metaxas.: Image Segmentation based on the Integration of Markov Random Fields and Deformable models. MICCAI (2000).

[19] Y. Chang and X. Li, "Adaptive image region-growing," *IEEE Transactions on Image Processing*, 3:868-872, 1994.

[20] C. Chu and J. Aggarwal, "The integration of image segmentation maps using region and edge information," *IEEE Transactions on Pattern Analysis and Machine Intelligence*, 15:1241-1252, 1993.

[21] S. Chu and A. Yuille, "Region competition: Unifying snakes, region growing and Bayes/MDL for multi-band image segmentation," *IEEE Transactions on Pattern Analysis and Machine Intelligence*, 18:884-900, 1996.

[22] M. Clark, L. Hall, D. Goldgof, L. Clarke, M. Silbiger and C. Li, "MRI segmentation using fuzzy clustering techniques: Integrating knowledge," *IEEE Engineering in Medicine and Biology Magazine*, 13:730-742, 1994.

[23] M. Clark, L. Hall, D. Goldgof, L. Clarke, R. Velthuizen, F. Murtagh and M. Silbiger, "Automatic tumor segmentation using knowledge-based techniques," *IEEE Transaction on Medical Imaging*, 17:187-201, 1998.

[24] L. Cohen, "On active contour models and balloons," *Computer Vision, Graphics, and Image Processing: Image Understanding*, 53:211-218, 1991.

[25] L. Cohen and I. Cohen, "Finite element methods for active contour models and balloons for 2D and 3D images," *IEEE Transactions on Pattern Analysis and Machine Intelligence*, 15:1131-1147, 1993.

[26] T. Cootes, G. Edwards and C. Taylor, "Active appearance models," *IEEE Transactions on Pattern Analysis and Machine Intelligence*, 23:681-685, 2001.

[27] T. Cootes, G. Edwards and C. Taylor, "Comparing active shape models with active appearance models," in T. Pridmore and D. Elliman (eds.) *British Machine Vision conference*, 1:173-182, 1999.

[28] T. Cootes, A. Hill, C. Taylor and J. Haslam, "The use of active shape models for locating structures in medical images," *Image and Vision Computing*, 12:355-366, 1994.

[29] T. Cootes, C. Taylor and D. Cooper, "Active shape models-their training and application," *Computer Vision and Image Understanding*, 61:38-59, 1995.

[30] T. Cover and P. Hart, "Nearest neighbor pattern classification," *IEEE Transaction on Information Theory*, 13:21-27, 1967.

[31] J. Cutrona and N. Bonnet, "Two methods for semi-automatic image segmentation based on fuzzy connectedness and watersheds," France-Iberic Microscopy Congress, Barcelona, 23-24, 2001.

[32] R. Duda and P. Hart, *Pattern Classification and Scene Analysis*, John Wiley & Sons, New York, 1973.

[33] N. Duta and M. Sonka, "Segmentation and interpretation of MR brain images: An improved active shape model," *IEEE Transactions on Medical Imaging*, 17:1049-1062, 1998.

[34] A. Falcao and J. Udupa, "Segmentation of 3D objects using live wire, in *Proceedings of Proceedings of SPIE*, 3034:228-239, 1997.

[35] A. Falcao, J. Udupa, S. Samarasekera, S. Sharma, B. Hirsch and R. Lotufo, "User-steered image segmentation paradigms: Live wire and live lane," *Graphical Models and Image Processing*, 60:233-260, 1998.

[36] A. Falcao, J. Udupa and F. Miyazawa, "An ultra-fast user-steered image segmentation paradigm: Live wire-on-the-fly," *IEEE Transactions on Medical Imaging*, 19:55-62, 2000.

[37] D. Fritsch, S. Pizer, L. Yu, V. Johnson, and E. Chaney,"Segmentation of Medical Image Objects using Deformable Shape Loci", *In International Conference on Information Processing in Medical Imaging*, pp. 127-140, Berlin, Germany, 1997. Springer-Verlag.

[38] S. Geman, D. Geman.: Stochastic relaxation, Gibbs distributions, and the Bayesian restoration of images. *IEEE Trans. Pattern Anal. Mach. Intell.* (6), pp.721-741, 1984.

[39] D. Geiger, A. Gupta, L. Costa and J. Vlontzos, "Dynamic programming for detecting, tracking, and matching deformable contours," IEEE Transactions on Pattern Analysis and Machine Intelligence, 17:294-302, 1995.

[40] A. Goldszal, C. Davatzikos, D. Pham, M. Yan, R. Bryan and S. Resnick, "An image-processing system for qualitative and quantitative volumetric analysis of brain images," *Journal of Computer Assisted Tomography*, 22:827-837, 1998.

[41] Gong,Y., Sakauchi, M.: Detection of Regions Matching Specified Chromatic Features, *Computer Vision and Image Understanding*, 61(2), p.263-269, 1995.

[42] L. Hall, A. Bensaid, L. Clarke, R. Velthuizen, M. Silbiger and J. Bezdek, "A comparison of neural network and fuzzy clustering techniques in segmenting magnetic resonance images of the brain," *IEEE Transaction no Neural Networks*, 3:672-682, 1992.

[43] G. Hamarneh and T. Gustavsson, "Combining snakes and active shape models for segmenting the human left ventricle in echocardiographic images," *IEEE Computers in Cardiology*, 27:115-118, 2000.

[44] R. Haralick and L. Shapiro, "Image segmentation techniques," *Computer Vision, Graphics, and Image Processing*, 29:100-132, 1985.

[45] I. L. Herlin, C. Nguyen, C. Graffigne, "A Deformable Region Model Using Stochastic Processes Applied to Echocardiographic Images", in *Proceedings of Conference of Computer Vision and Pattern Recognition (CVPR'92)*, 534-539, Urbana, IL, June, 1992.

[46] G. Herman and B. Carvalho, "Multiseeded segmentation using fuzzy connectedness," *IEEE Transactions on Pattern Analysis and Machine Intelligence*, 23:460-474, 2001.

[47] R. Herndon, J. Lancaster, A. Toga and P. Fox, "Quantification of white matter and gray matter volumes from T1 parametric images using fuzzy classifiers," *Journal of Magnetic Resonance Imaging*, 6:425-435, 1996.

[48] G. Hillman, C. Chang, H. Ying and J. Yen, "Automatic system for brain MRI analysis using a novel combination of fuzzy rule-based and

automatic clustering techniques," in imiitProceedings of SPIE, 16-25, 1995.

[49] J. Jin, C. Imielinska, A.F. Laine, J. Udupa, W. Shen, S.B. Heymsfield, "Segmentation and Evaluation of Adipose Tissue from Whole Body MRI Scans", MICCAI 2003 Conference, Montreal, CA.

[50] C. Imielinska, P. Molholt, "The Vesalius ProjectTM - Could it be a Revolution in Medical Education?", *CACM*, in print.

[51] Imielinska, C.; Downes, M; and Yuan, W., "Semi-Automated Color Segmentation of Anatomical Tissue", Journal of Computerized Medical Imaging and Graphics, 24(2000), 173-180, April, 2000.

[52] Imielinska, C., Laino-Pepper, L., Thumann, R., Villamil, R., "Technical Challenges of 3DVisualization of Large Color Data Sets", in the *Proceedings of the Second User Conference of the NLM's Visible Human Project*, Oct. 1998, Bethesda, MD.

[53] Imielinska, C.; Metaxas, D.; Udupa, J.; Jin, Y.; Chen, T., "Hybrid Segmentation of the Visible Human Data", in the Proceedings of the Third Visible Human Project Conference, Bethesda, MD, Oct. 2000.

[54] C. Imielinska, D. Metaxas, J. Udupa, Y. Jin and T. Chen, "Hybrid segmentation of Anatomical Data," in *Proceedings of MICCAI2001*, 1048-1057, 2001.

[55] Y. Jin, C. Imielinska, A. Laine, "A Homogeneity-Based Speed Term for Level-set Shape Detection", *SPIE Medical Imaging*, San Diego, 2002.

[56] T. Jones, *Image-Based Ventricular Blood Flow Analysis*, Doctoral Dissertation, University of Pennsylvania, 1998.

[57] T. Jones and D. Metaxas, "Automated 3D segmentation using deformable models and fuzzy affinity," in *Proceedings of Information Processing in Medical Imaging*, 113-126, 1997.

[58] Jones, T., Metaxas D,: Image Segmentation based on the Integration of Pixel Affinity and Deformable Models, *Proc. IEEE CVPe*, Santa Barbara, CA, June 1998.

[59] M. Kass, A. Witkin and D. Terzopoulos, "Snakes: Active contour models," *International Journal of Computer Vision*, 1:321-331, 1987.

[60] C. Li and C. Lee, "Minimum entropy thresholding," *Pattern Recognition*, 26:617-625, 1993.

[61] H. Liu, "Two- and Three-dimensional boundary detection," *Computer Graphic Processing*, 6:123-134, 1977.

[62] S. Lobreg and M. Viergever, "A discrete dynamic contour model," *IEEE Transactions on Medical Imaging*, 14:12-24, 1995.

[63] R. Malladi, J. Sethian and B. Vemuri, "Shape modeling with front propagation: A level set approach," *IEEE Transactions on Pattern Analysis and Machine Intelligence*, 17:158-175, 1995.

[64] T. McInerney and D. Terzopoulos, "A dynamic finite element surface model for segmentation and tracking in multidimensional medical images with application to cardiac 4D image analysis," *Computerized Medical Imaging and Graphics*, 19:69-83, 1995.

[65] T. McInerney and D. Terzopoulos, "Deformable models in medical image analysis: A survey," *Medical Image Analysis*, 1:91-108, 1996.

[66] D.N. Metaxas, Physics-Based Deformable Models: Application to Computer Vision, Graphics, and Medical Imaging, 1996.

[67] S. Mitchell, B. Lelieveldt, R. Geest, J. Reiber and M. Sonka, "Multistage hybrid active appearance model matching: Segmentation of left and right ventricles in cardiac MR images," *IEEE Transactions on Medical Imaging*, 20:415-423, 2001.

[68] F. Mohamed, S. Vinitski, S. Faro, C. Gonzalez, J. Mack and T. Iwanaga, "Optimization of tissue segmentation of brain MR images based on multispectral 3D feature map," *Magnetic Resonance Imaging*, 17:403-409, 1999.

[69] U. Montanari, "On the optimal detection of curves in noisy pictures," *Communications of the ACM*, 14:335-345, 1971.

[70] Morgenthaler and A. Rosenfeld, "Multidimensional edge detection by hypersurface fitting," *IEEE Transactions on Pattern Analysis and Machine Intelligence*, 3:482-486, 1981.

[71] E. Mortensen and W. Barrett, "Intelligent scissors for image composition," in *Proceedings of Computer Graphics (SIGGRAPH'95)*, 191-198, 1995.

[72] W. Neuenschwander, P. Fua, G. Szekely and O. Kubler, "Initializing snakes," in *Proceedings* of CVPR, 658-663, 1994.

[73] L. Nyul and J. Udupa: "On Standardizing the MR Image Intensity Scale," *Magnetic Resonance in Medicine*, 42:1072-1081, 1999.

[74] S. Osher and J. Sethian, "Fronts propagating with curvature-dependent speed: Algorithms based on Hamilton-Jacobi formulations," *Journal of Computational Physics*, 79:12-49, 1988.

[75] N. Otsu, "A threshold selection method from gray-level histograms," *IEEE Transaction on Systems, Man, and Cybernetics*, 9:62-66, 1979.

[76] N. Pal and S. Pal, "A review on image segmentation techniques," *Pattern Recognition*, 26:1277-1294, 1993.

[77] N. Paragios and R. Deriche, "Geodesic active contours and level sets for the detection and tracking of moving objects," *IEEE Transactions on Pattern Analysis and Machine Intelligence*, 22:266-280, 2000.

[78] N. Paragios and R. Deriche, "Geodesic active region: a new framework to deal with frame partition problems in computer vision," *Journal of Visual Communication and Image Representation*, 13:249-268, 2002.

[79] N. Paragios and R. Deriche, "Geodesic active region and level set methods for supervised texture segmentation," *International Journal of Computer Vision*, 46:223-247, 2002.

[80] J. Park and J. Keller, "Snakes on the Watershed," IEEE Transactions on Pattern Analysis and Machine Intelligence, 23:1201-1205, 2001.

[81] T. Pavlidis and Y. Liow, "Integrating region growing and edge detection," *IEEE Transactions on Pattern Analysis and Machine Intelligence*, 12:225-233, 1990.

[82] X. Pei and M. Gabbouj, "Robust image contour detection by watershed transformation," in Proceedings of IEEE Workshop on Nonlinear Signal and Image Processing, 315-319, 1997.

[83] M. Penedo, M. Carreira, A. Mosquera and D. Cabello, "Computer-aided diagnosis: a neural-network-based approach to lung nodule detection," *IEEE Transaction on Medical Imaging*, 17:872-880, 1998.

[84] D. Pham and J. Prince, "Adaptive fuzzy segmentation of magnetic resonance images," *IEEE Transaction on Medical Imaging*, 18:737-752, 1999.

[85] D. Pham, "Spatial models for fuzzy clustering," *Computer Vision and Image Understanding*, 84:285-297, 2001.

[86] D. Pham, J. Prince, A. Dagher and C. Xu, "An automated technique for statistical characterization of brain tissue in magnetic resonance imaging", *International Journal on Pattern Recognition and Artificial Intelligence*, 11:1189-1211, 1997.

[87] D. Pham, C. Xu and J. Prince, "Current methods in medical image segmentation," *Annual Review Biomedical Engineering*, 2:315-337, 2000.

[88] T. Pong, L. Shapiro, L. Watson and R. Haralick, "Experiments in segmentation using facet model region grower," *Computer Vision, Graphics, and Image Processing*, 25:1-23, 1984.

[89] D. Pope, D. Parker, D. Gustafson and P. Clayton, "Dynamic search algorithms in left ventricular border recognition and analysis of coronary arteries," *IEEE Proceedings of Computers in Cardiology*, 9:71-75, 1984.

[90] C. Poon and M. Braun, "Image segmentation by a deformable contour model incorporating region analysis," *Physics in Medicine and Biology*, 42:1833-1841, 1997.

[91] Preparata, F.P.; Shamos, M.I.: *Computational Geometry*, New York, Springer, 1985.

[92] J. Prewitt and M. Mendelsohn, "The analysis of cell images," *Annals of the New York Academy of Science*, 128:1035-1053, 1966.

[93] W. Reddick, J. Glass, E. Cook, T. Elkin and R. Deaton, "Automated segmentation and classification of multispectral magnetic resonance images of brain using artificial neural networks, *IEEE Transaction on Medical Imaging*, 16:911-918, 1997.

[94] R. Ronfard, "Region-based strategies for active contour models," *International Journal of Computer Vision*, 13:229-251, 1994.

[95] K. Saarinen, "Color image segmentation by a watershed algorithm region adjacency graph processing," in *Proceedings of ICIP*, 1021-1025, 1994.

[96] P. Saha, J. Udupa and D. Odhner, "Scale-based fuzzy connected image segmentation: Theory, algorithms and validation," *Computer Vision and Image Understanding*, 77:145-174, 2000.

[97] P. Saha and J. Udupa, "Relative fuzzy connectedness among multiple objects: Theory, algorithms, and applications in image segmentation," *Computer Vision and Image Understanding*, 82:42-56, 2001.

[98] P. Saha and J. Udupa, "Fuzzy connected object delineation: Axiomatic path strength definition and the case of multiple seeds," *Computer Vision and Image Understanding*, 83:275-295, 2001.

[99] P. Saha and J. Udupa, "Optimum image thresholding via class uncertainty and region homogeneity," *IEEE Transactions on Pattern Analysis and Machine Intelligence*, 23:689-706, 2001

[100] P. Saha and J. Udupa, "Iterative relative fuzzy connectedness and object definition: Theory, algorithms, and applications in image segmentation," in *Proceedings of IEEE Workshop on Mathematical Methods in Biomedical Image Analysis*, 28-35, 2000.

[101] P. Saha, J. Udupa and R. Lotufo, "Relative fuzzy connectedness and object definition: Theory, algorithms, and applications in image segmentation," *IEEE Transactions on Pattern Analysis and Machine Intelligence*, 24, 1485-1500, 2002.

[102] B. Sahiner, H. Chan, N. Petrick, D. Wei, M. Helvie, D. Adler and M. Goodsitt, "Classification of mass and normal breast tissue: a convolution neural network classifier with spatial domain and texture images," *IEEE Transaction on Medical Imaging*, 15:598-610, 1996.

[103] P. Sahoo, S. Soltani and A. Wong, "A survey of thresholding techniques," *Computer Vision, Graphics, and Image Processing*, 41: 233-260, 1988.

[104] P. Salembier and M. Pardas, "Hierarchical morphological segmentation for image sequence coding," *IEEE Transactions on Image Processing*, 3:639-651, 1994.

[105] A. Schenk, G. Prause and H. Peitgen, "Local cost computation for efficient segmentation of 3D objects with live wire," in *Proceedings of SPIE*, 4322:1357-1364, 2001.

[106] J. Sethian, *Level Set Methods*, Cambridge University Press, 1996.

[107] J. Sethian, *Level set methods and fast marching methods*, 1999.

[108] L. Shafarenko, M. Petrou and J. Kittler, "Automatic watershed segmentation of randomly textured color images," *IEEE Transactions on Image Processing*, 6:1530-1544, 1997.

[109] K. Siddiqi, Y. Lauziere, A. Tannenbaum and W. Zucker, "Area and length minimizing flows for shape segmentation," *IEEE Transactions on Image Processing*, 7:433-443, 1998.

[110] Spitzer, V., Ackerman, M.J., Scherzinger, A.L., Whitlock, D.: The Visible Human Male: A Technical Report, JAMIA, 3(2), pp.118-130 1996.

[111] M. Trivedi and J. Bezdek, "Low-level segmentation of aerial images with fuzzy clustering," *IEEE Transaction on Systems, Man, and Cybernetics*, 16:589-598, 1986.

[112] J. Udupa, "Interactive segmentation and boundary surface formation for 3D digital images," *Computer Graphics and Image Processing*, 18:213-235, 1982.

[113] Udupa, J.K., Samarasekera, S.: Fuzzy Connectedness and Object Definition, In *SPIE Proceedings*, vol.2431, pp. 2-11, 1995.

[114] J. Udupa and S. Samarasekera, "Fuzzy connectedness and object definition: Theory, algorithms, and applications in image segmentation," *Graphical Models and Image Processing*, 58:246-261, 1996.

[115] Udupa, J.K., Leblanc, V.R., Schmidt, H., Imielinska, C., Saha, K.P., Grevera G.J., Zhuge, Y., Molholt, P., Currie L., Jin, Y., A Methodology for Evaluating Image Segmentation Algorithms", SPIE 2002.

[116] R. Urquhart, "Graph theoretical clustering based on limited neighborhood sets," *Pattern Recognition*, 15:173-187, 1982.

[117] O. Veksler, "Image segmentation by nested cut," in *Proceedings of CVPR*, 1:339-344, 2000.

[118] Z. Wu and R. Leahy, "An optimal graph theoretic approach to data clustering: theory and its application to image segmentation," *IEEE Transactions on Pattern Analysis and Machine Intelligence*, 15:1101-1113, 1993.

[119] C. Xu and J. Prince, "Snakes, shapes, and gradient vector flow," *IEEE Transaction on Image Processing*, 7:359-369, 1998.

[120] Y. Zhu and Z. Yan, "Computerized tumor boundary detection using a Hopfield neural network," *IEEE Transaction on Medical Imaging*, 16:55-67, 1997.

[121] Y. Zhuge and J. Udupa, "Vectorial scale-based fuzzy connected image segmentation," in *Proceedings of SPIE*, 4684:1476-1487, 2002.

[122] S. Zucker, "Region growing: childhood and adolescence," *Computer Graphics Image Processing*, 5:382-399, 1976.

[123] Kaufmann, A.: Introduction to the Theory of Fuzzy Subsets, Vol. I, Academic Press, New York, 1975.

[124] Lorensen, W.E., and Cline, H.E., "Marching Cubes: A High Resolution 3D Surface Construction Algorithm", *Computer Graphics: A Quarterly Report of SIGGRAPH-ACM* 21(4), pp.163-168, 1987.

[125] T. Chen, "Integration of Gibbs Prior Models, Marching Cubes Methods and Deformable Models in Medical Image Segmentation"', Ph.D. dissertation, University of Pennsylvania, May 2003.

[126] R. Whitaker, Volumetric Deformable Models, in *Proceedings of the Third Conference on Visualization in Biomedical Computing* (VBC'94), Rochester, MN, October, 1994.

[127] D. Terzopoulos, Regularization of Inverse Visual Problems Involving Discontinuities. *IEEE Transaction on Pattern Analysis and Machine Intelligence*, 8(4): 413-424, 1986.

[128] T. McInerney and D. Terzopoulos, A Dynamic Finite Element Surface Model for Segmentation and Tracking in Multidimensional Medical Images with Application to Cardiac 4D Image Analysis. *Computerized Medical Imaging and Graphics* 19(1): 69-83, 1995.

[129] L. H. Staib, J. S. Duncan, Deformable Fourier Models for Surface Finding in 3D Images, in Proceedings of the Second Conference on Visualization in Biomedical Computing (VBC'92), Chapel Hill, NC, October, 1992, volume 1808 of *SPIE Proceedings*, 90-104.

[130] L. H. Staib, J. S. Duncan, Boundary Finding with Parametrically Deformable Models, *IEEE Transaction on Pattern Analysis and Machine Intelligence* 14(11): 1061-1075, 1992.

[131] R. Malladi, J. Sethian, B. C. Vemuri, Shape Modeling with Front Propagation: A Level Set Approach, *IEEE Transaction on Pattern Analysis and Machine Intelligence* 17(2): 158-175.

[132] T. Chan and L. Vese, Active Contours without Edges, IEEE Transaction on Image Processing, 10(2) pp: 266-277, 2001.

[133] A. Yezzi, S. Kichenssamy, A. Kumar, P. Olver, and A. Tannebaum, A Geometric Snake Model for Segmentation of Medical Imagery, IEEE Tansaction on Medical Imaging, 16(2) pp: 199-209, 1997.

[134] C. Xu and J. L. Prince, Generalized Gradient Vector Flow External Forces for Active Contours, Signal Processing: An International Journal, 71(2), pp. 131-139, December 1998.

[135] C. Montani, R. Scateni, R. Scopigno, Discretized Marching Cubes, In: Bergeron, R. D. and Kaufman, A. E., editors, Proceedingss of the Visualization '94 Congress, 1994, IEEE Computer Society Press, pp. 281-287.

[136] William E. Lorensen, Harvey E. Cline. Marching cubes: A high-resolution 3D surface construction algorithm. Proceedingss of the 14th

annual conference on Computer graphics and interactive techniques. Pages: 163 - 169